Available online at www.sciencedirect.com
SCIENCE DIRECT
Engineering Fracture Mechanics 73 (2006) 1292–1320
Engineering Fracture Mechanics
www.elsevier.com/locate/engfracmech

Stress intensity factors of an inclined elliptical crack near a bimaterial interface

Nao-Aki Noda *, Takao Kouyama, Yositomo Kinoshita

Department of Mechanical Engineering, Kyushu Institute of Technology, 1-1, Sensui-cho, Tobata, Kitakyushu 804-8550, Japan

Received 7 February 2005; received in revised form 2 January 2006; accepted 9 January 2006
Available online 31 March 2006

Abstract

In this paper the stress intensity factors are discussed for an inclined elliptical crack near a bimaterial interface. The solution utilizes the body force method and requires Green's functions for perfectly bonded semi-infinite bodies. The formulation leads to a system of hypersingular integral equation whose unknowns are three modes of crack opening displacements. In the numerical calculation, unknown body force densities are approximated by using fundamental density functions and polynomials. The results show that the present method yields smooth variations of stress intensity factors along the crack front accurately. Distributions of stress intensity factors are presented in tables and figures with varying the shape of crack, distance from the interface, and elastic modulus ratio. It is found that the inclined crack can be evaluated by the models of vertical and parallel cracks within the error of 24% even for the cracks very close to the interface.

Keywords: Elasticity; Crack; Bimaterial; Interface; Elliptical crack; Stress intensity factor; Body force method

1. Introduction

The structural strength of composite materials is controlled to a considerable extent by the size, shape, orientation, and distribution of the flaws and imperfections, which exist in the material. With increasing use of composite materials in engineering structure, much attention has been paid to the strength of interface. Although a lot of researches have been made in terms of fracture mechanics approach regarding interface, most of them generally involve two-dimensional modeling [1–3]. Little work has been carried out on the three-dimensional model aspect of crack problems except those of specially shaped cracks [4–10]. This is mainly due to the extreme difficulties of solving such problems in terms of mathematics and mechanics, or to the substantial computation required in the numerical analyses.

Considering such a situation, the authors previously analyzed an elliptical crack parallel to an interface using the body force method coupled with hypersingular integral equation formulation. Then, the stress intensity factors were calculated with varying the elastic modulus ratio and geometrical parameters systematically

* Corresponding author. Tel./fax: +81 93 884 3124.
E-mail address: noda@mech.kyutech.ac.jp (N.-A. Noda).

0013-7944/$ - see front matter
doi:10.1016/j.engfracmech.2006.01.018

Nomenclature

a	major radius of an elliptical crack $[(x/a)^2+(y/b)^2=1]$
b	minor radius of an elliptical crack $[(x/a)^2+(y/b)^2=1]$
h	distance between crack and interface
φ	inclination angle of crack (see Fig. 1)
β	parametric angle of ellipse $[x=a\cos\beta,\ y=b\sin\beta,\ \beta=\tan^{-1}((ay)/(bx))]$
(x,y,z)	rectangular coordinate
(ξ,η,ζ)	rectangular coordinate (x,y,z) where the body force is applied
E_1, E_2	elastic modulus for space 1 and space 2
μ_1, μ_2	shear modulus for space 1 and space 2
ν_1, ν_2	Poisson's ratio for space 1 and space 2
$w_{zz}(\xi_a,\eta_b)$, $w_{yz}(\xi_a,\eta_b)$, $w_{zx}(\xi_a,\eta_b)$	fundamental body force densities to express the stress fields due to an elliptical crack in an infinite body under uniform tension and shears $\sigma_z^\infty, \tau_{yz}^\infty, \tau_{zx}^\infty$
$f_{zz}(\xi,\eta)$, $f_{yz}(\xi,\eta)$, $f_{zx}(\xi,\eta)$	unknown body force densities
(u_x,u_y,u_z)	displacement in (x,y,z) direction
$U_x(x,y)$	crack opening displacement $=u_x(x,y,+0)-u_x(x,y,-0)$
$U_y(x,y)$	crack opening displacement $=u_y(x,y,+0)-u_y(x,y,-0)$
$U_z(x,y)$	crack opening displacement $=u_z(x,y,+0)-u_z(x,y,-0)$
K_{I}, K_{II}, K_{III}	stress intensity factors
F_{I}, F_{II}, F_{III}	dimensionless stress intensity factors normalized by $\sigma\sqrt{\pi b}$
F_{I}^*	dimensionless stress intensity factors normalized by $\sigma\sqrt{\pi\sqrt{\mathrm{area}}}$
area	πab. However, if $b/a\leqslant 0.2$, area $=20b^2$
$\hat{F}_{\mathrm{IA}}$	stress intensity factor at A of an inclined crack defined by Eq. (8)
F_{IA}^0	stress intensity factor at A of a projected crack, $\varphi=0^\circ$
F_{IA}^0	stress intensity factor at A of a projected crack, $\varphi=90^\circ$

[11]. Also, they analyzed a rectangular crack terminating a bimaterial interface, and proposed stress intensity formulas [12–14]. However, since actual cracks or defects are usually inclined to an interface, errors should be estimated when the crack is approximated as parallel or vertical cracks. In this study, first, the stress intensity factor will be considered for an elliptical crack vertical to an interface. Second, an inclined elliptical crack near in interface as shown in Fig. 1 will be analyzed. Third, the results for inclined crack and the ones for the parallel and vertical cracks will be compared when the projected area of the inclined crack is equal to the area of the parallel and vertical cracks.

In the previous studies using the body force method, Noguchi et al. [15] and Oda et al. [16] treated an elliptical crack near a free surface, but the this paper deals with more general case of the crack near an interface with varying the elastic modulus ratio. Lee et al. [7] analyzed the crack on the interface ($h=0$ in Fig. 1) and the vertical crack near the interface ($h\neq 0$ and $\varphi=0$ in Fig. 1), but this paper treat the case of $h\neq 0$ and $\varphi=0$ in Fig. 1.

In the present analysis, the problems will be expressed as a system of hypersingular integral equations on the idea of the body force method. Then, the unknown body force densities will be approximated as the products of fundamental densities and polynomials. The present solution yields accurate and smooth distributions of mixed mode stress intensity factors, which is usually difficult to be obtained by using other analyses [11–13,17,18].

2. Method of analysis

Consider an elliptical crack near a bimaterial interface, under uniform tension σ_z^∞, σ_y^∞ at infinity as shown in Fig. 1. Here, the elliptical crack has principal diameters $2a$ and $2b$. The body force method is used to formulate the problem as a system of singular integral equations (1), whose unknowns are body force densities

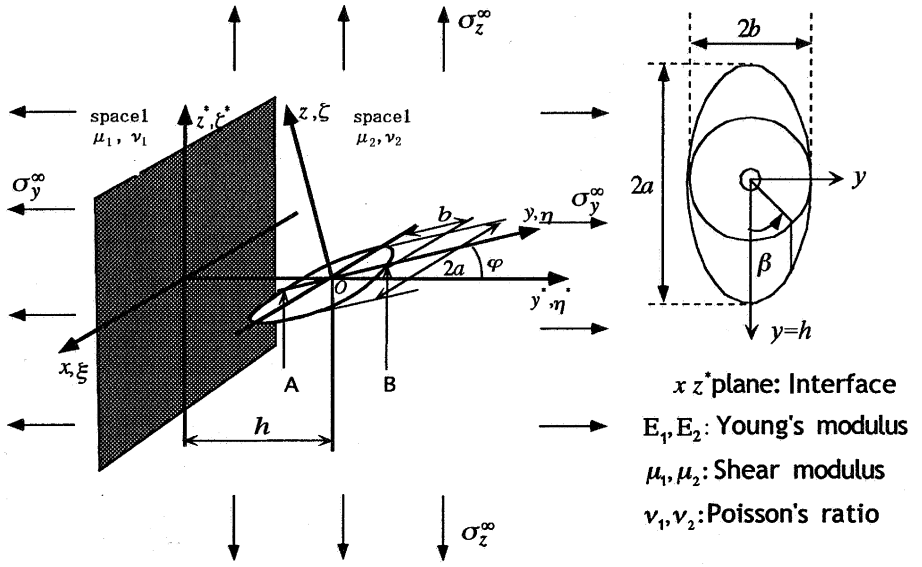

Fig. 1. An inclined elliptical crack near a bimaterial interface ($x^2/a^2 + y^2/b^2 = 1$).

$f_{zz}(\xi,\eta), f_{yz}(\xi,\eta), f_{zx}(\xi,\eta)$. The body force densities are equivalent to crack opening displacements as shown in Eq. (1e). Here, (ξ,η,ζ) is a (x,y,z) coordinate where the body force is applied.

$$\left.\begin{aligned}&\frac{(1-2\nu)}{8\pi(1-\nu)^2}\left[\iint_S \frac{f_{zz}(\xi,\eta)}{r_1^3}\,\mathrm{d}\xi\,\mathrm{d}\eta\right.\\&\quad\left.+\int\int_s K_{zz}^{f_{zz}}(\xi,\eta,x,y,\varphi)f_{zz}(\xi,\eta)\,\mathrm{d}\xi\,\mathrm{d}\eta\right]\\&\quad+\tfrac{1}{8\pi(1-\nu)}\left[\int\int_s K_{zz}^{f_{yz}}(\xi,\eta,x,y,\varphi)f_{yz}(\xi,\eta)\,\mathrm{d}\xi\,\mathrm{d}\eta\right.\\&\quad\left.+\int\int_s K_{zz}^{f_{zx}}(\xi,\eta,x,y,\varphi)f_{zx}(\xi,\eta)\,\mathrm{d}\xi\,\mathrm{d}\eta\right]=-(\sigma_z^\infty\cos^2\varphi+\sigma_y^\infty\sin^2\varphi)\end{aligned}\right\}\tag{1a}$$

$$\left.\begin{aligned}&\frac{1}{8\pi(1-\nu)}\left[\iint_S \frac{6\nu(x-\xi)(y-\eta)}{r_1^5}f_{yz}(\xi,\eta)\,\mathrm{d}\xi\,\mathrm{d}\eta\right.\\&\quad+\iint_S\left\{\frac{2(1-2\nu)}{r_1^3}+\frac{6\nu(y-\eta)^2}{r_1^5}\right\}f_{zx}(\xi,\eta)\,\mathrm{d}\xi\,\mathrm{d}\eta\\&\quad+\int\int_s K_{yz}^{f_{zz}}(\xi,\eta,x,y,\varphi)f_{zz}(\xi,\eta)\,\mathrm{d}\xi\,\mathrm{d}\eta+\int\int_s K_{yz}^{f_{yz}}(\xi,\eta,x,y,\varphi)f_{yz}(\xi,\eta)\,\mathrm{d}\xi\,\mathrm{d}\eta\\&\quad\left.+\int\int_s K_{yz}^{f_{zx}}(\xi,\eta,x,y,\varphi)f_{zx}(\xi,\eta)\,\mathrm{d}\xi\,\mathrm{d}\eta\right]=(\sigma_y^\infty-\sigma_z^\infty)\cos\varphi\sin\varphi\end{aligned}\right\}\tag{1b}$$

$$\left.\begin{aligned}&\frac{1}{8\pi(1-\nu)}\left[\iint_S\left\{\frac{2(1-2\nu)}{r_1^3}+\frac{6\nu(x-\xi)^2}{r_1^5}\right\}f_{yz}(\xi,\eta)\,\mathrm{d}\xi\,\mathrm{d}\eta\right.\\&\quad+\iint_S \frac{6\nu(x-\xi)(y-\eta)}{r_1^5}f_{zx}(\xi,\eta)\,\mathrm{d}\xi\,\mathrm{d}\eta\\&\quad+\int\int_s K_{zx}^{f_{zz}}(\xi,\eta,x,y,\varphi)f_{zz}(\xi,\eta)\,\mathrm{d}\xi\,\mathrm{d}\eta+\int\int_s K_{zx}^{f_{yz}}(\xi,\eta,x,y,\varphi)f_{yz}(\xi,\eta)\,\mathrm{d}\xi\,\mathrm{d}\eta\\&\quad\left.+\int\int_s K_{zx}^{f_{zx}}(\xi,\eta,x,y,\varphi)f_{zx}(\xi,\eta)\,\mathrm{d}\xi\,\mathrm{d}\eta\right]=0\end{aligned}\right\}\tag{1c}$$

$$\left.\begin{aligned}&y=y^*/\cos\varphi,\quad z=z^*/\cos\varphi\\&r_1=\sqrt{(x-\xi)^2+(y^*-\eta^*)^2+(z^*-\zeta^*)^2}\\&S=\{(\xi,\eta)(\xi/a)^2+(\eta/b)^2\leqslant 1\}\end{aligned}\right\}\tag{1d}$$

$$\left.\begin{aligned}
U_z(x,y) &= u_z(x,y,+0) - u_z(x,y,-0) \\
&= \frac{(1-2\nu_1)(1+\nu_1)}{E_1(1-\nu_1)} f_{zz}(x,y), \\
U_y(x,y) &= u_y(x,y,+0) - u_y(x,y,-0) \\
&= \frac{2(1+\nu_1)}{E_1} f_{yz}(x,y), \\
U_x(x,y) &= u_x(x,y,+0) - u_x(x,y,-0) \\
&= \frac{2(1+\nu_1)}{E_1} f_{zx}(x,y)
\end{aligned}\right\} \tag{1e}$$

In Eq. (1e), E_1, E_2 are elastic modulus, and ν_1, ν_2 are Poisson's ratio for space 1 and space 2. Eqs. (1a), (1b), (1c) enforce boundary conditions at the prospective boundary S for crack; that is, $\sigma_z = 0$, $\tau_{yz} = 0$, $\tau_{zx} = 0$. Eq. (1) includes singular terms in the form of $1/r^3$, $1/r^5$ corresponding to the ones of an elliptical crack in an infinite body. Therefore the integration $\fint\!\!\!\fint_S$ should be interpreted in a sense of a finite part integral [19] in the region S. As an example, the notation $K_{zz}^{f_{zz}}(\xi,\eta,x,y)$ refers to a function that satisfies the boundary condition for bimaterial interface. In the conventional body force method, the crack region is divided into several elements; then, fundamental density functions and step functions were used to approximate unknown functions. However, the use of step functions gives rise to singularities along the element boundaries, and it tends to deteriorate the accuracy and validity in sophisticated problems. In the present analysis, the following expressions have been used to approximate the unknown functions as continuous functions.

$$\left.\begin{aligned}
f_{zz}(\xi,\eta) &= F_{zz}(\xi_a,\eta_b) w_{zz}(\xi_a,\eta_b) \\
f_{yz}(\xi,\eta) &= F_{yz}(\xi_a,\eta_b) w_{yz}(\xi_a,\eta_b) \\
f_{zx}(\xi,\eta) &= F_{zx}(\xi_a,\eta_b) w_{zx}(\xi_a,\eta_b) \\
w_{zz}(\xi_a,\eta_b) &= \frac{4(1-\nu)^2 b\sigma_z^\infty}{(1-2\nu)E(k)} \sqrt{1-\xi_a^2-\eta_b^2} \\
w_{yz}(\xi_a,\eta_b) &= \frac{2b(1-\nu)k^2\tau_{yz}^\infty}{C(k)} \sqrt{1-\xi_a^2-\eta_b^2} \\
w_{zx}(\xi_a,\eta_b) &= \frac{2b(1-\nu)k^2\tau_{zx}^\infty}{B(k)} \sqrt{1-\xi_a^2-\eta_b^2} \\
B(k) &= (k^2-\nu)E(k) + \nu k'^2 K(k) \\
C(k) &= (k^2+\nu k'^2)E(k) - \nu k'^2 K(k) \\
K' &= b/a \leqslant 1, \quad k = \sqrt{1-(b/a)^2}, \quad \xi_a = \xi/a, \quad \eta_b = \eta/b \\
K(k) &= \int_0^{\pi/2} \frac{\mathrm{d}\lambda}{\sqrt{1-k^2\sin^2\lambda}} \\
E(k) &= \int_0^{\pi/2} \sqrt{1-k^2\sin^2\lambda}\,\mathrm{d}\lambda
\end{aligned}\right\} \tag{2}$$

Here, $w_{zz}(\xi_a,\eta_b)$, $w_{yz}(\xi_a,\eta_b)$, $w_{zx}(\xi_a,\eta_b)$ are called a fundamental density function of body force, which express the stress field due to an elliptical crack in an infinite body under uniform tension and shears σ_x^∞, τ_{yz}^∞, τ_{zx}^∞ and leads to solutions with high accuracy [20]. In this calculation, we can put $\sigma_z^\infty = \tau_{yz}^\infty = \tau_{zx}^\infty = 1$. Since the problem is symmetric to the x and y axis, the following expressions (3) can be applied to approximate three unknown functions $F_{zz}(\xi_a,\eta_b)$, $F_{yz}(\xi_a,\eta_b)$, $F_{zx}(\xi_a,\eta_b)$.

$$
\left.\begin{aligned}
F_{zz}(\xi_a,\eta_b) &= \alpha_0\xi_a^0\eta_b^0+\alpha_1\xi_a^0\eta_b^1+\cdots+\alpha_{n-1}\xi_a^0\eta_b^{n-1}+\alpha_n\xi_a^0\eta_b^n\\
&\quad+\alpha_{n+1}\xi_a^2\eta_b^0+\alpha_{n+2}\xi_a^2\eta_b^1+\cdots+\alpha_{2n-1}\xi_a^2\eta_b^{n-1}\\
&\qquad\vdots\qquad\vdots\\
&\quad+\alpha_l\xi_a^{2\cdot n}\\
&=\sum_{i=0}^{l}\alpha_i G_i(\xi_a,\eta_b),\\
F_{yz}(\xi_a,\eta_b) &= \beta_0\xi_a^0\eta_b^0+\beta_1\xi_a^0\eta_b^1+\cdots+\beta_{n-1}\xi_a^0\eta_b^{n-1}+\beta_n\xi_a^0\eta_b^n\\
&\quad+\beta_{n+1}\xi_a^2\eta_b^0+\beta_{n+2}\xi_a^2\eta_b^1+\cdots+\beta_{2n}\xi_a^2\eta_b^{n-1}\\
&\qquad\vdots\qquad\vdots\\
&\quad+\beta_l\xi_a^{2\cdot n}\\
&=\sum_{i=0}^{l}\beta_i G_i(\xi_a,\eta_b),\\
F_{zx}(\xi_a,\eta_b) &= \gamma_0\xi_a\eta_b^0+\gamma_1\xi_a\eta_b^1+\cdots+\gamma_{n-1}\xi_a\eta_b^{n-1}+\gamma_n\xi_a\eta_b^n\\
&\quad+\gamma_{n+1}\xi_a^3\eta_b^0+\gamma_{n+2}\xi_a^3\eta_b^1+\cdots+\gamma_{2n}\xi_a^3\eta_b^{n-1}\\
&\qquad\vdots\qquad\vdots\\
&\quad+\gamma_1\xi_a^{2\cdot n+1}\eta_b^0\\
&=\sum_{i=0}^{l}\gamma_i Q_i(\xi_a,\eta_b),\ l=\frac{(n+1)(n+2)}{2}.
\end{aligned}\right\}
\tag{3}
$$

$$
\left.\begin{aligned}
&G_0(\xi_a,\eta_b)=1, G_1(\xi_a,\eta_b)=\eta_b,\dots\\
&\qquad\dots, G_{n+1}(\xi_a,\eta_b)=\xi_a^2,\dots, G_l(\xi_a,\eta_b)=\xi_a^{2\cdot n},\\
&Q_0(\xi_a,\eta_b)=\xi_a, Q_1(\xi_a,\eta_b)=\xi_a\eta_b\dots\\
&\qquad\dots, Q_{n+1}(\xi_a,\eta_b)=\xi_a^3,\dots, Q_{l-1}(\xi_a,\eta_b)=\xi_a^{2\cdot n+1}
\end{aligned}\right\}
\tag{4}
$$

Using the approximation method mentioned above, we obtain the following system of algebraic equations for the determination of unknown coefficients $\alpha_0\sim\alpha_i$, $\beta_0\sim\beta_i$, $\gamma_0\sim\gamma_i$ $[i=1,2,\dots,1,1=(1/2)(n+1)(n+2)]$, which can be determined by selecting a set of collocation points.

$$
\left.\begin{aligned}
&\sum_{i=0}^{l}[\alpha_i(A_{zz,i}^{f_{zz}}+B_{zz,i}^{f_{zz}})+\beta_i\beta_{zz,i}^{f_{yz}}+\gamma_iB_{zz,i}^{f_{zx}}]=-(\sigma_z^\infty\cos^2\varphi+\sigma_y^\infty\sin^2\varphi)\\
&\sum_{i=0}^{l}[\alpha_iB_{yz,i}^{f_{zz}}+\beta_i(A_{yz,i}^{f_{yz}}+B_{yz,i}^{f_{yz}})+\gamma_i(A_{yz,i}^{f_{zx}}+B_{yz,i}^{f_{zx}})]=(\sigma_y^\infty-\sigma_z^\infty)\sin\varphi\cos\varphi\\
&\sum_{i=0}^{l}[\alpha_iB_{zx,i}^{f_{zz}}+\beta_i(A_{zx,i}^{f_{yz}}+B_{zx,i}^{f_{yz}})+\gamma_i(A_{zx,i}^{f_{zx}}+B_{zx,i}^{f_{zx}})]=0
\end{aligned}\right\}
\tag{5a}
$$

The number of unknowns in Eq. (5a) is 3 (1 + 1). As examples, $A_{zz,i}^{f_{zz}}$, $B_{zz,i}^{f_{zz}}$, $B_{zz,i}^{f_{yz}}$, $B_{zz,i}^{f_{zx}}$ are expressed as follows:

$$
\left.\begin{aligned}
A_{zz,i}^{f_{zz}} &= \frac{b}{2\pi E(k)}\fint\!\!\!\fint_s\frac{G_i(\xi_a,\eta_b)}{r^3}\sqrt{1-\xi_a^2-\eta_b^2}\,\mathrm{d}\xi\,\mathrm{d}\eta\\
B_{zz,i}^{f_{zz}} &= \frac{b}{8\pi E(k)}\int\!\!\int_s K_{zz}^{f_{zz}}(\xi,\eta,x,y)G_i(\xi_a,\eta_b)\sqrt{1-\xi_a^2-\eta_b^2}\,\mathrm{d}\xi\,\mathrm{d}\eta\\
B_{zz,i}^{f_{yz}} &= \frac{bk^2}{8\pi C(k)}\int\!\!\int_s K_{zz}^{f_{yz}}(\xi,\eta,x,y)Q_i(\xi_a,\eta_b)\sqrt{1-\xi_a^2-\eta_b^2}\,\mathrm{d}\xi\,\mathrm{d}\eta\\
B_{zz,i}^{f_{zx}} &= \frac{bk^2}{8\pi B(k)}\int\!\!\int_s K_{zx}^{f_{zx}}(\xi,\eta,x,y)R_i(\xi_a,\eta_b)\sqrt{1-\xi_a^2-\eta_b^2}\,\mathrm{d}\xi\,\mathrm{d}\eta
\end{aligned}\right\}
\tag{5b}
$$

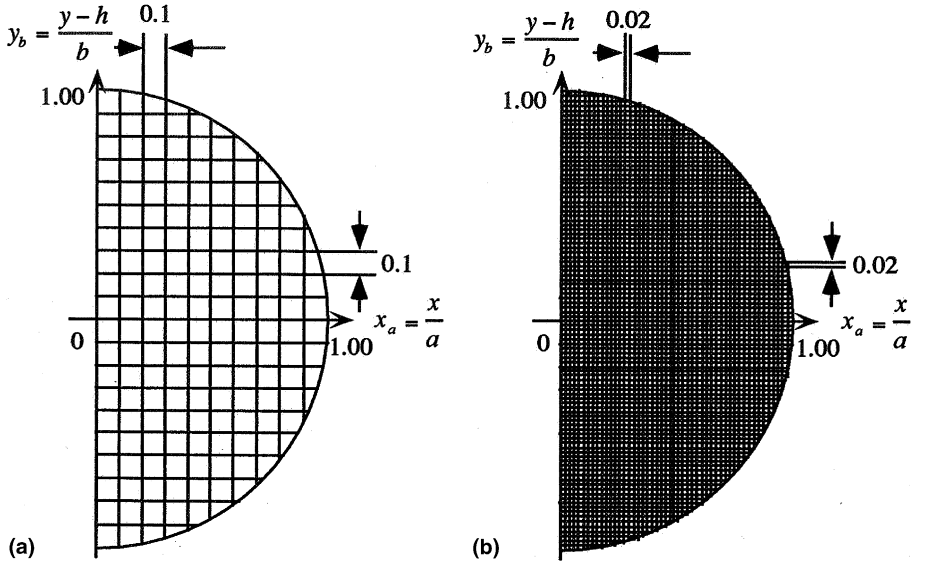

Fig. 2. Boundary collocation points: (a) 10×20, (b) 50×100.

In Eq. (5b) the integral $B^{f_{zz}}_{zz,i}$ can be evaluated numerically because of no singularities in the integral. However $A^{f_{zz}}_{zz,i}$ cannot be evaluated by ordinary numerical procedure because they have hypersingularities of the form r^{-3} when $x = \xi$ and $y = \eta$ [19] . Therefore a similar method of as shown in previous papers is applied [17,18] . Fig. 2 shows boundary collocation points.

The boundary conditions are considered at the intersection of themeshonthe (x_a, y_b) plane in the region of $x_a^2 + y_a^2 < 1,\ x_a \geqslant 0$, where $x_a = x/a$, $y_b = y/b$. Fig. 2(a) shows 10×20 mesh whose width is 0.1, and Fig. 2(b) shows 50×100 mesh whose width is 0.02.

3. Numerical results and discussion

3.1. Dimensionless stress intensity factors

Numerical calculations have been carried out for various n in Eqs. (3), (4) when $a/b = 1, 2, \infty$ and ν_1, $\nu_2 = 0.3$. Numerical integrals have been performed using scientific subroutine library (FACOM SSL II DAQE etc.). In demonstrating the numerical results of stress intensity factors K_{I}, K_{II}, K_{III} the following dimensionless factors F_{I}, F_{II}, F_{III} will be used.

$$\left.\begin{aligned} F_{\mathrm{I}}(\beta) &= \frac{K_{\mathrm{I}}(\beta)}{\sigma_z^{\infty}\sqrt{\pi b}} = \frac{F_{zz}}{E(k)}\left[\sin^2\beta + \left(\frac{b}{a}\right)^2\cos^2\beta\right]^{1/4} \\ F_{\mathrm{II}}(\beta) &= \frac{K_{\mathrm{II}}(\beta)}{\sigma_z^{\infty}\sqrt{\pi b}} = \left(F_{zx}\frac{k'\cos\beta}{B(k)} + F_{yz}\frac{\sin\beta}{C(k)}\right)\frac{k^2}{(1-k^2\cos^2\beta)^{1/4}} \\ F_{\mathrm{III}}(\beta) &= \frac{K_{\mathrm{III}}(\beta)}{\sigma_z^{\infty}\sqrt{\pi b}} = \left(-F_{zx}\frac{\sin\beta}{B(k)} + F_{yz}\frac{k'\cos\beta}{C(k)}\right)\frac{(1-\nu)k^2}{(1-k^2\cos^2\beta)^{1/4}} \end{aligned}\right\} \tag{6}$$

3.2. Convergence and accuracy of the results

Tables 1 and 2 show convergence of stress intensity factors $F_{\mathrm{I}}(\beta)$, $F_{\mathrm{II}}(\beta)$ at $\beta = \pi/2$, $3\pi/2$ when $a/b = 2$, the elastic shear modulus ratio $\mu_2/\mu_1 = 0$, ∞, Poisson's ratio ν_1, $\nu_2 = 0.3$ and $\varphi = 15°$, $75°$. Table 1 has

Table 1
Convergence of the results F_{IA}, F_{IIA}, F_{IB}, F_{IIB} when $\mu_2/\mu_1 = 0, \infty$, $\beta = \pi/2, 3\pi/2$, ν_1, $\nu_2 = 0.3$ with the collocation points 10×20 (see Fig. 2(a)): (a) $\varphi = 15°$, (b) $\varphi = 75°$

h/b	n	F_{IA}		F_{IIA}		F_{IB}		F_{IIB}	
		$\mu_2/\mu_1 = 0$	$\mu_2/\mu_1 = \infty$	$\mu_2/\mu_1 = 0$	$\mu_2/\mu_1 = \infty$	$\mu_2/\mu_1 = 0$	$\mu_2/\mu_1 = \infty$	$\mu_2/\mu_1 = 0$	$\mu_2/\mu_1 = \infty$
(a)									
	8	0.9677	0.5488	0.2853	0.1357	0.9358	0.4672	0.2020	0.1899
1.2	9	0.9680	0.5483	0.2853	0.1352	0.9354	0.4676	0.2020	0.1896
	10	0.9685	0.5398	0.2854	0.1349	0.9357	0.4674	0.2021	0.1897
	8	0.8740	0.6351	0.2494	0.1408	0.8596	0.5955	0.2047	0.1985
1.4	9	0.8741	0.6350	0.2493	0.1408	0.8596	0.5956	0.2047	0.1985
	10	0.8741	0.6350	0.2494	0.1408	0.8596	0.5956	0.2047	0.1985
	8	0.8010	0.7243	0.2277	0.2034	0.7972	0.7165	0.2136	0.2421
2.0	9	0.8010	0.7243	0.2277	0.2034	0.7972	0.7165	0.2136	0.2421
	10	0.8010	0.7243	0.2277	0.2034	0.7972	0.7165	0.2136	0.2421
(b)									
	8	1.0168	0.5480	−0.2847	−0.1193	0.9826	0.5613	0.2931	0.1204
1.2	9	1.0171	0.5476	−0.2848	−0.1190	0.9823	0.5616	0.2931	0.1203
	10	1.0174	0.5471	−0.2848	−0.1188	0.9821	0.5616	0.2932	0.1203
	8	0.9511	0.6297	−0.2624	−0.1210	0.9407	0.6354	0.2754	0.1296
1.4	9	0.9512	0.6296	−0.2623	−0.1210	0.9407	0.6353	0.2754	0.1296
	10	0.9512	0.6296	−0.2624	−0.1210	0.9406	0.6354	0.2754	0.1296
	8	0.8528	0.7229	−0.2353	−0.1645	0.8482	0.7125	0.2486	0.1632
2.0	9	0.8528	0.7229	−0.2353	−0.1645	0.8482	0.7125	0.2486	0.1632
	10	0.8528	0.7229	−0.2353	−0.1645	0.8482	0.7125	0.2486	0.1632

Table 2
Convergence of the results F_{IA}, F_{IIA}, F_{IB}, F_{IIB} when $\mu_2/\mu_1 = 0,\infty$, $\beta = \pi/2, 3\pi/2$, ν_1, $\nu_2 = 0.3$ with the collocation points 50×100 (see Fig. 2(b)): (a) $\varphi = 15°$, (b) $\varphi = 75°$

h/b	n	F_{IA}		F_{IIA}		F_{IB}		F_{IIB}	
		$\mu_2/\mu_1 = 0$	$\mu_2/\mu_1 = \infty$	$\mu_2/\mu_1 = 0$	$\mu_2/\mu_1 = \infty$	$\mu_2/\mu_1 = 0$	$\mu_2/\mu_1 = \infty$	$\mu_2/\mu_1 = 0$	$\mu_2/\mu_1 = \infty$
(a)									
	13	1.2346	0.4066	0.3022	0.0974	1.1235	0.3895	0.2543	0.1186
1.05	14	1.2350	0.4062	0.3021	0.0973	1.1234	0.3896	0.2544	0.1184
	15	1.2354	0.4059	0.3021	0.0972	1.1237	0.3899	0.2543	0.1185
	13	1.1176	0.4631	0.2942	0.1126	0.9852	0.4124	0.2402	0.1372
1.1	14	1.1180	0.4627	0.2943	0.1128	0.9854	0.4126	0.2403	0.1372
	15	1.1182	0.4624	0.2942	0.1129	0.9855	0.4126	0.2403	0.1374
(b)									
	13	1.3970	0.3768	−0.3247	−0.0873	1.1762	0.3597	0.3646	0.1076
1.05	14	1.3975	0.3770	−0.3247	−0.0872	1.1765	0.3599	0.3645	0.1077
	15	1.3979	0.3771	−0.3248	−0.0873	1.1767	0.3541	0.3645	0.1076
	13	1.1728	0.4506	−0.3020	−0.1097	1.0038	0.4368	0.3397	0.1381
1.1	14	1.1731	0.4509	−0.3021	−0.1098	1.0040	0.4370	0.3398	0.1380
	15	1.1734	0.4512	−0.3021	−0.1098	1.0041	0.4371	0.3398	0.1381

convergence to the fourth digit when $h/b \geqslant 1.2$ with 10×20 boundary collocation points as shown in Fig. 2(a). Table 2 has convergence to the fourth digit when $h/b = 1.05$ with 50×100 boundary collocation points as shown in Fig. 2(b). In the following calculation, therefore, the collocation points of 10×20 will be used when $h/b \geqslant 1.2$, and the ones of 50×100 will be used when $h/b \leqslant 1.1$. In the previous papers [11–13,17,18], more detail discussions may be found for the accuracy of the numerical solutions using polynomial and fundamental density approximations.

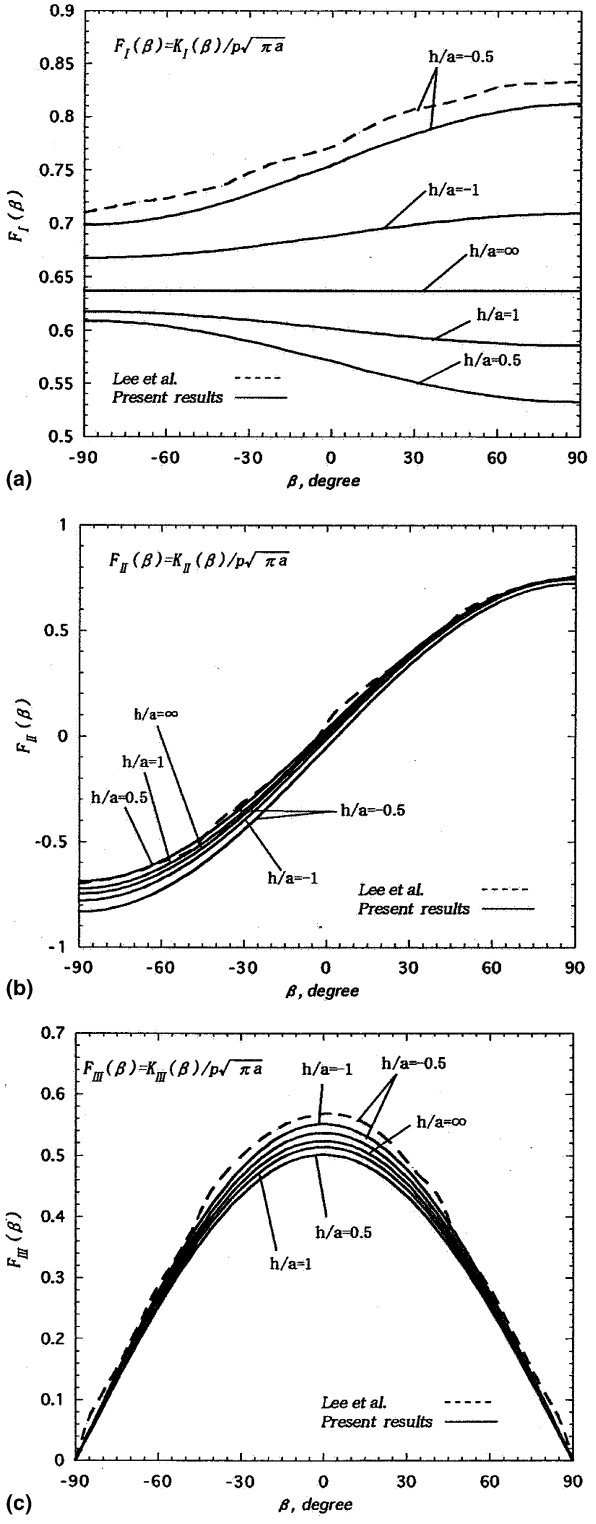

Fig. 3. Variations of stress intensity factors for parallel, penny-shaped crack, under internal shear and normal loading when $a/b = 1$, $\mu_2 = 3$, ν_1, $\nu_2 = 0.3$, $\tau_{zx} = -p$, $\sigma_{zz} = -p$ in Fig. 1: (a) K_1 vs. β, (b) K_{II} vs. β, (c) K_{III} vs. β.

Table 3
Dimensionless stress intensity factors F_{IA}, F_{IB}, F^*_{IA}, F^*_{IB} when ν_1, $\nu_2 = 0.3$ in Fig. 4

h/b	a/b	F_{IA}				F^*_{IA}				F_{IB}				F^*_{IB}			
		$\mu_2/\mu_1 = 0$	$\mu_2/\mu_1 = 0.5$	$\mu_2/\mu_1 = 2$	$\mu_2/\mu_1 = \infty$	$\mu_2/\mu_1 = 0$	$\mu_2/\mu_1 = 0.5$	$\mu_2/\mu_1 = 2$	$\mu_2/\mu_1 = \infty$	$\mu_2/\mu_1 = 0$	$\mu_2/\mu_1 = 0.5$	$\mu_2/\mu_1 = 2$	$\mu_2/\mu_1 = \infty$	$\mu_2/\mu_1 = 0$	$\mu_2/\mu_1 = 0.5$	$\mu_2/\mu_1 = 2$	$\mu_2/\mu_1 = \infty$
1.05	1	0.9066	0.7120	0.5680	0.4381	0.6810	0.5348	0.4266	0.3291	0.6560	0.6423	0.6314	0.6213	0.4927	0.4824	0.4743	0.4667
	2	1.3781	0.9654	0.7070	0.4999	0.8704	0.6098	0.4466	0.3157	0.8935	0.8439	0.8095	0.7797	0.5644	0.5330	0.5113	0.4925
	∞	2.1551	1.2334	0.8212	0.5387	1.0194	0.5830	0.3883	0.2547	1.2544	1.0562	0.9552	0.8803	0.5930	0.4994	0.4517	0.4163
	$(a/b = 1)/(a/b = \infty)$	0.4207	0.5773	0.6917	0.8133	0.6680	0.9173	1.0986	1.2921	0.5230	0.6081	0.6610	0.7058	0.8309	0.9660	1.0500	1.1211
1.1	1	0.8071	0.6863	0.5901	0.4989	0.6062	0.5155	0.4432	0.3747	0.6535	0.6416	0.6320	0.6229	0.4909	0.4819	0.4747	0.4679
	2	1.1859	0.9230	0.7394	0.5799	0.7490	0.5830	0.4670	0.3663	0.8842	0.8419	0.8111	0.7838	0.5585	0.5318	0.5123	0.4951
	∞	1.7583	1.1712	0.8616	0.6283	0.8313	0.5537	0.4074	0.2971	1.2111	1.0503	0.9590	0.8883	0.5726	0.4965	0.4535	0.4201
	$(a/b = 1)/(a/b = \infty)$	0.4590	0.5860	0.6849	0.7940	0.7292	0.9310	1.0879	1.2612	0.5396	0.6109	0.6590	0.7012	0.8573	0.9706	1.0467	1.1138
1.2	1	0.7331	0.6653	0.6094	0.5550	0.5507	0.4997	0.4577	0.4169	0.6500	0.6406	0.6329	0.6255	0.4882	0.4812	0.4754	0.4698
	2	1.0408	0.8866	0.7699	0.6627	0.6574	0.5600	0.4863	0.4186	0.8715	0.8388	0.8137	0.7909	0.5505	0.5298	0.5139	0.4995
	∞	1.4621	1.1136	0.9029	0.7278	0.6914	0.5266	0.4270	0.3442	1.1659	1.0411	0.9654	0.9033	0.5513	0.4923	0.4565	0.4271
	$(a/b = 1)/(a/b = \infty)$	0.5014	0.5974	0.6749	0.7626	0.7965	0.9489	1.0719	1.2112	0.5575	0.6153	0.6556	0.6925	0.8855	0.9775	1.0414	1.1000
1.25	1	0.7135	0.6596	0.6147	0.5709	0.5359	0.4954	0.4617	0.4288	0.6487	0.6402	0.6332	0.6265	0.4873	0.4809	0.4756	0.4706
	2	1.0016	0.8761	0.7791	0.6886	0.6326	0.5534	0.4921	0.4349	0.8669	0.8376	0.8148	0.7939	0.5476	0.5290	0.5146	0.5014
	∞	1.3847	1.0983	0.9153	0.7605	0.6548	0.5194	0.4328	0.3596	1.1467	1.0375	0.9676	0.9086	0.5422	0.4906	0.4575	0.4297
	$(a/b = 1)/(a/b = \infty)$	0.5153	0.6006	0.6716	0.7507	0.8184	0.9538	1.0668	1.1924	0.5657	0.6171	0.6544	0.6895	0.8987	0.9802	1.0396	1.0952
1.3	1	0.6994	0.6554	0.6187	0.5826	0.5253	0.4923	0.4647	0.4376	0.6476	0.6399	0.6335	0.6274	0.4864	0.4806	0.4758	0.4713
	2	0.9729	0.8683	0.7861	0.7087	0.6145	0.5484	0.4965	0.4476	0.8630	0.8317	0.8157	0.7965	0.5451	0.5253	0.5152	0.5031
	∞	1.3297	1.0855	0.9251	0.7866	0.6288	0.5133	0.4375	0.3720	1.1326	1.0346	0.9697	0.9138	0.5356	0.4892	0.4585	0.4321
	$(a/b = 1)/(a/b = \infty)$	0.5260	0.6038	0.6688	0.7407	0.8354	0.9591	1.0622	1.1763	0.5718	0.6185	0.6533	0.6866	0.9081	0.9824	1.0377	1.0907

1.4	1	0.6806	0.6499	0.6239	0.5985	0.5112	0.4882	0.4686	0.4495	0.6457	0.6393	0.6340	0.6289	0.4850	0.4802	0.4762	0.4724
	2	0.9337	0.8573	0.7961	0.7379	0.5897	0.5415	0.5028	0.4661	0.8566	0.8347	0.8173	0.8010	0.5410	0.5272	0.5162	0.5059
	∞	1.2535	1.0676	0.9399	0.8264	0.5927	0.5048	0.4445	0.3908	1.1118	1.0299	0.9734	0.9233	0.5257	0.4870	0.4603	0.4366
	$(a/b=1)/(a/b=\infty)$	0.5430	0.6087	0.6638	0.7242	0.8625	0.9671	1.0542	1.1502	0.5808	0.6207	0.6513	0.6811	0.9226	0.9860	1.034S	1.0820
1.6	1	0.6615	0.6441	0.6295	0.6152	0.4969	0.4838	0.4728	0.4621	0.6431	0.6386	0.6348	0.6311	0.4830	0.4797	0.4768	0.4740
	2	0.8904	0.8449	0.8077	0.7719	0.5624	0.5337	0.5102	0.4875	0.8478	0.8322	0.8196	0.8077	0.5355	0.5256	0.5177	0.5102
	∞	1.1670	1.0460	0.9683	0.8774	0.5518	0.4946	0.4579	0.4149	1.0840	1.0231	0.9790	0.9384	0.5126	0.4838	0.4629	0.4437
	$(a/b=1)/(a/b=\infty)$	0.5668	0.6158	0.6501	0.7012	0.9005	0.9782	1.0325	1.1138	0.5933	0.6242	0.6484	0.6725	0.9423	0.9915	1.0300	1.0683
1.8	1	0.6522	0.6413	0.6322	0.6232	0.4899	0.4817	0.4749	0.4681	0.6414	0.6381	0.6352	0.6325	0.4818	0.4793	0.4771	0.4751
	2	0.8681	0.8383	0.8138	0.7901	0.5483	0.5295	0.5140	0.4990	0.8421	0.8306	0.8212	0.8122	0.5319	0.5246	0.5187	0.5130
	∞	1.1200	1.0336	0.9691	0.9082	0.5296	0.4888	0.4583	0.4295	1.0661	1.0185	0.9830	0.9495	0.5041	0.4816	0.4648	0.4490
	$(a/b=1)/(a/b=\infty)$	0.5823	0.6205	0.6524	0.6862	0.9250	0.9855	1.0362	1.0899	0.6016	0.6265	0.6462	0.6661	0.9558	0.9952	1.0265	1.0581
2.0	1	0.6470	0.6397	0.6336	0.6277	0.4860	0.4805	0.4759	0.4715	0.6403	0.6377	0.6356	0.6335	0.4809	0.479	0.4774	0.4758
	2	0.8551	0.8345	0.8174	0.8010	0.5401	0.5271	0.5163	0.5059	0.8382	0.8294	0.8222	0.8153	0.5294	0.5239	0.5193	0.5150
	∞	1.0909	1.0258	0.9761	0.9285	0.5159	0.4851	0.4616	0.4391	1.0536	1.0152	0.9859	0.9579	0.4982	0.4801	0.4662	0.4530
	$(a/b=1)/(a/b=\infty)$	0.5931	0.6236	0.6491	0.6760	0.9420	0.9905	1.0310	1.0738	0.6077	0.6282	0.6447	0.6613	0.9653	0.9977	1.0240	1.0503
∞	1	0.6366	0.6366	0.6366	0.6366	0.4782	0.4782	0.4782	0.4782	0.6366	0.6366	0.6366	0.6366	0.4782	0.4782	0.4782	0.4782
	2	0.8257	0.8257	0.8257	0.8257	0.5215	0.5215	0.5215	0.5215	0.8257	0.8257	0.8257	0.8257	0.5215	0.5215	0.5215	0.5215
	∞	1.0000	1.0000	1.0000	1.0000	0.4729	0.4729	0.4729	0.4729	1.0000	1.0000	1.0000	1.0000	0.4729	0.4729	0.4729	0.4729
	$(a/b=1)/(a/b=\infty)$	0.6366	0.6366	0.6366	0.6366	1.0112	1.0112	1.0112	1.0112	0.6366	0.6366	0.6366	0.6366	1.0112	1.0112	1.0112	1.0112

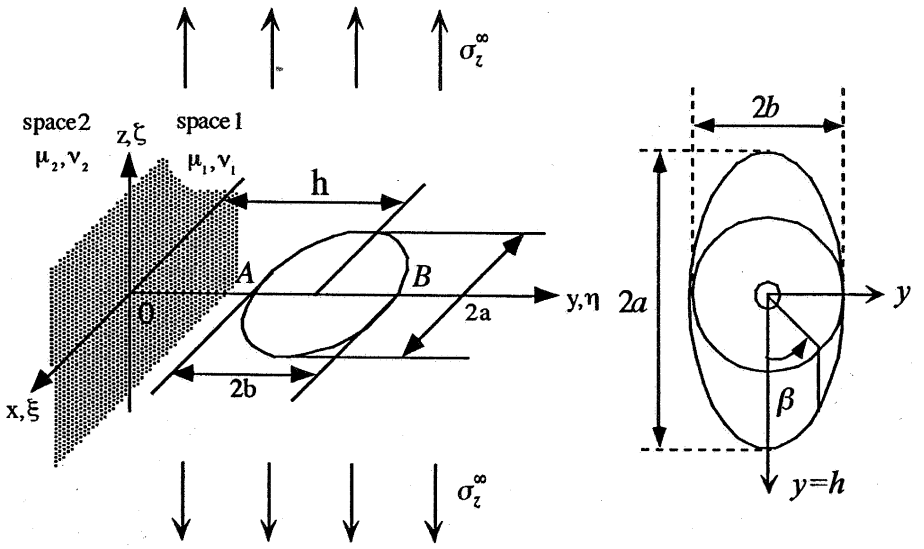

Fig. 4. An elliptical crack vertical to a bimaterial interface $(x^2/a^2 + (y-h)^2/b^2 = 1)$.

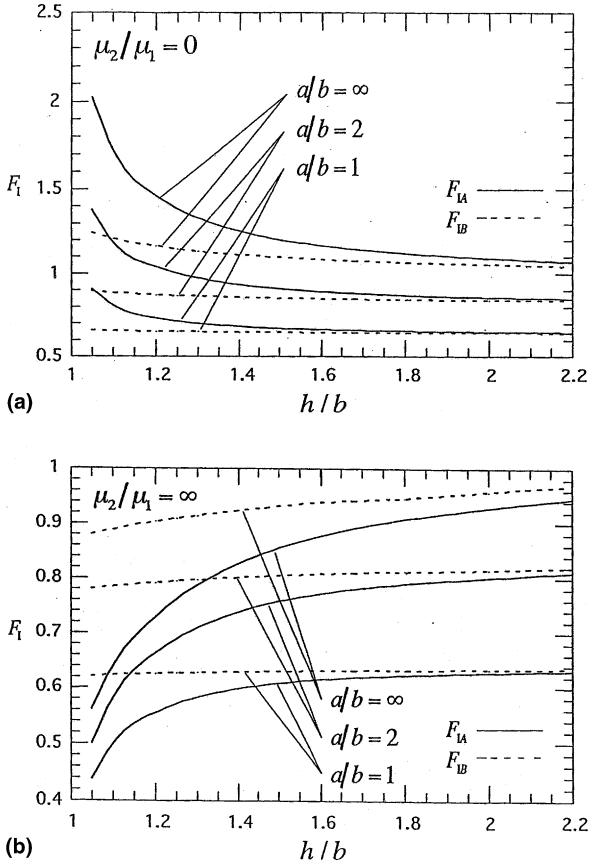

Fig. 5. F_{IB}, F_{IA} vs. h/b in Fig. 4 with ν_1, $\nu_2 = 0.3$: (a) when $\mu_2/\mu_1 = 0$, (b) when $\mu_2/\mu_1 = \infty$.

3.3. Results of an elliptical crack parallel to an interface

In this study, first, the stress intensity factors for a parallel crack to an interface are analyzed. Then, it is confirmed that the present results are coincide with the previous ones [11]. Another examples of a parallel crack are examined in Fig. 3. Fig. 3(a)–(c) show the distributions of the stress intensity factors of an elliptical crack parallel to an interface under internal shear and normal loading when $a/b = 1$, μ_2, $\mu_1 = 3$, ν_1, $\nu_2 = 0.3$. The results of Lee–Farris–Keer [7] are indicated as dotted lines. If the results of $h/a = c_1$ and $h/a = -c_1$ (c_1 is a positive constant) are compared, the absolute values are always larger when $h/a = -c_1$, that is, when the crack is in material 2, whose shear modulus $\mu_2 = 3$. However, F_{II} values in [7] have different tendency. It is found that the results of [7] have the largest error by 16% when $\beta = -90°$ in Fig. 3(b). The results of Lee et al. [7] have about 16% deviations at most when $\beta = -90°$ in Fig. 3(b). It is seen that the present results are indicated as smooth curves because unknown functions are approximated as polynomials . The detail results for a parallel crack are indicated in [11].

3.4. Results of an elliptical crack vertical to an interface

Table 3 indicates mode I stress intensity factors for a crack vertical to an interface at $\beta = \pi/2$, $\beta = 3\pi/2$ when $\mu_2/\mu_1 = 0$, 0.5, 2, ∞, $a/b = 1$, 2, ∞, and $h/b = 1.05$ to ∞ (see Fig. 4). Here, the following dimensionless stress intensity factor is also indicated [21].

$$F_{\mathrm{I}}^{*} = \frac{K_{\mathrm{I}}}{\sigma_z^{\infty}\sqrt{\pi\sqrt{\mathrm{area}}}} = \left(\frac{b}{\pi a}\right)^{1/4} \times F_{\mathrm{I}} \tag{7}$$

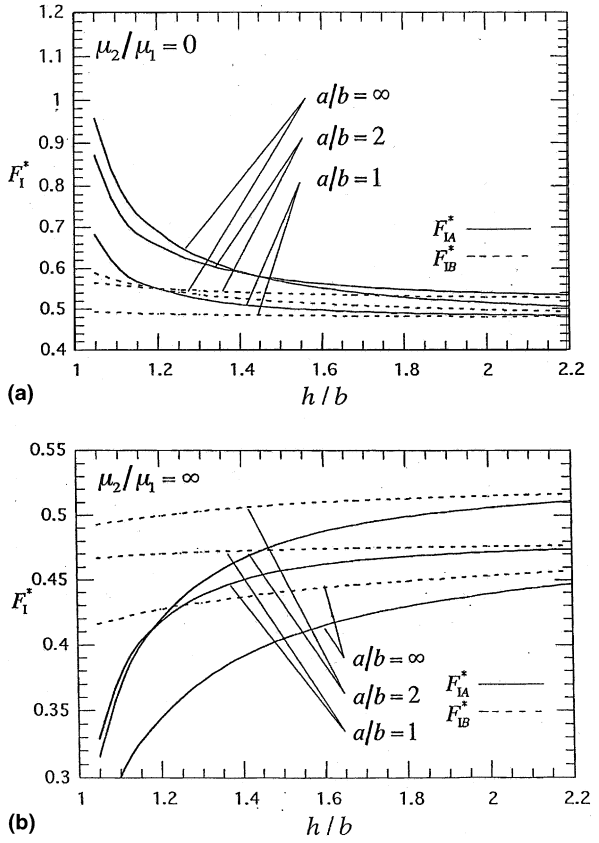

Fig. 6. F_{IB}^{*}, F_{IA}^{*} vs. h/b in Fig. 4 when $\mu_2/\mu_1 = 0$ with ν_1, $\nu_2 = 0.3$: (a) when $\mu_2/\mu_1 = 0$, (b) when $\mu_2/\mu_1 = \infty$.

Here, area $= \pi ab$. However, if $b/a \leqslant 0.2$, area $= 20b^2$. The notation $(a/b = 1)/(a/b = \infty)$ denotes the ratio of the results of $a/b = 1$ to the ones of $a/b = \infty$. It is seen that when $h/b = 1.05$ the ratio of F_{I} is in the range 0.45–0.78, but the ratio of F_1^*, is in the range 0.71–1.241 $\cong 1$. In other words, the effect of aspect ratio is small for F_1^*, and therefore the expression may be useful for engineering applications. Fig. 5 shows the relationship between F_{IB}, F_{IA} and h/b when $\mu_2/\mu_1 = 0, \infty$, and Fig. 6 shows the relationship between F_{IB}^*, F_{IA}^* and h/b when $\mu_2/\mu_1 = 0, \infty$. It is seen that F_{IB}^*, F_{IA}^* are insensitive to the crack aspect ratio.

Fig. 7 shows the distributions of F_{I} when $a/b = 1, 2$, $h/b = 1.2$, ν_1, $\nu_2 = 0.3$ with varying μ_2, $\mu_1 = 0$ to ∞. Fig. 8 is the ones when $a/b = 1$, $\mu_2/\mu_1 = 0, \infty$, ν_1, $\nu_2 = 0.3$, with varying $h/b = 1.05$ to ∞. Also, Fig. 9 is the ones when $a/b = 2$, $\mu_2/\mu_1 = 0, \infty$, ν_1, $\nu_2 = 0.3$ with varying $h/b = 1.05$ to ∞. As shown in Fig. 7(a), compared with the homogeneous case $\mu_2/\mu_1 = 1$, F_{I} value of $\mu_2/\mu_1 = 0$ is larger by 15.2%, but F_{I} value of $\mu_2/\mu_1 = \infty$ is smaller by 12.8%. Similarly, F_{I} value of $\mu_2/\mu_1 = 0.5$ is larger by 4.5%, but F_{I}, value of $\mu_2/\mu_1 = 2$ is smaller by 4.3%. Similar trends can be seen in Figs. 7(b), 8, 9. The results in Figs. 7–9 indicate that the F_{I} shows a non-regular behavior at $\beta = 270°$ as $h/b \to 1$ because the elliptical crack is touching the interface at this point. The present numerical solution gives sooth distributions of stress intensity factors because unknown body forces densities are approximated as polynomial forms instead of step-functions [17].

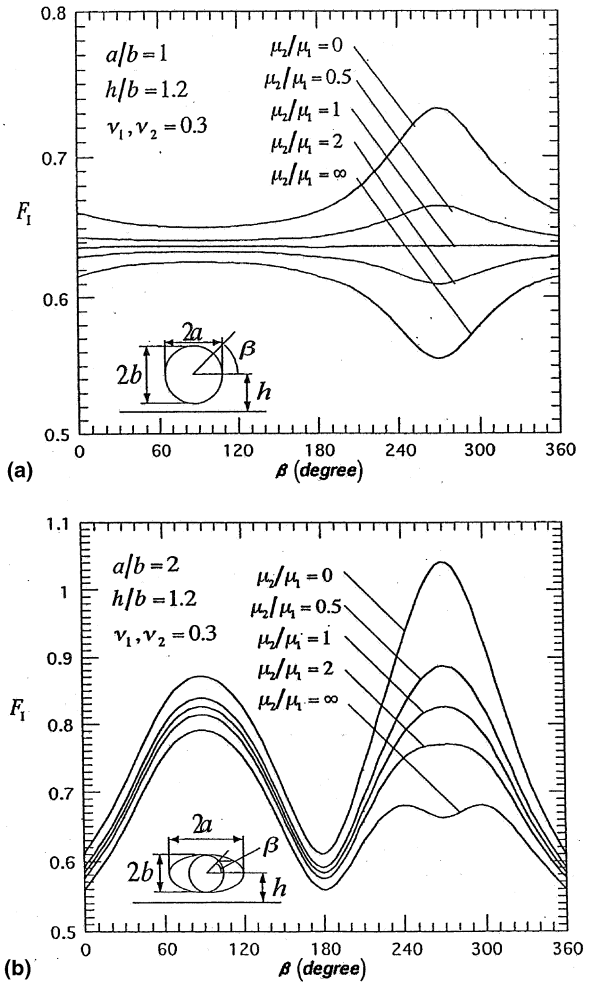

Fig. 7. Variation of $F_{\mathrm{I}}(\beta)$ in Fig. 4 with $h/b = 1.2$, ν_1, $\nu_2 = 0.3$: (a) when $a/b = 1$, (b) when $a/b = 2$.

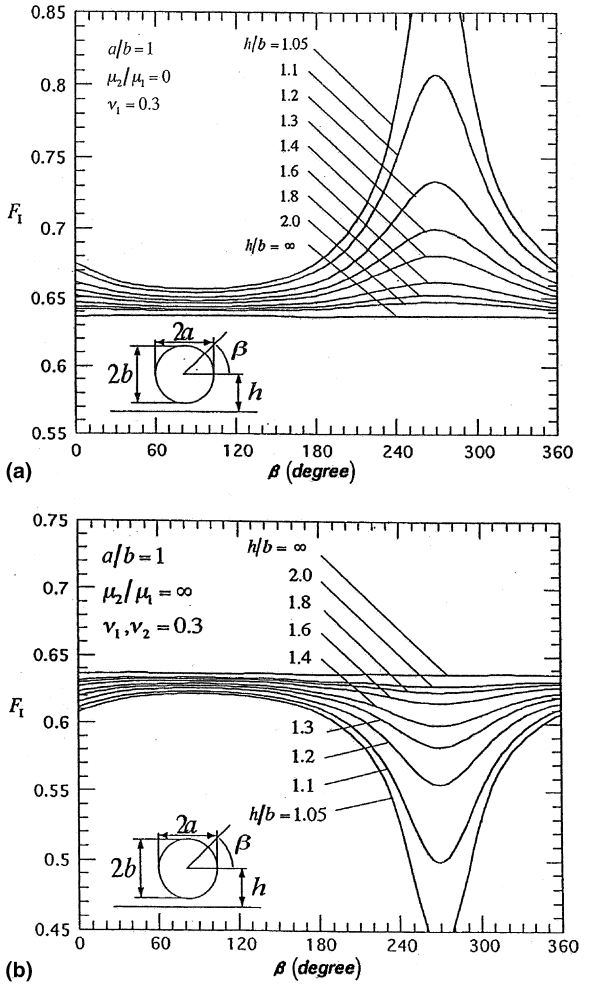

Fig. 8. Variation of $F_{\mathrm{I}}(\beta)$ in Fig. 4 with $a/b = 1$, ν_1, $\nu_2 = 0.3$: (a) when $\mu_2/\mu_1 = 0$, (b) when $\mu_2/\mu_1 = \infty$.

3.5. Results of an inclined elliptical crack near an interface

In this study, an inclined crack is considered under remote tension parallel or vertical to the interface as shown in Fig. 10.

Tables 4–7 show the results at $\beta = 3\pi/2$ when $\mu_2/\mu_1 = 0$, ∞, and $a/b = 1$, 2, ∞ with varying $h/b = 1.05$ to ∞. In these Tables, $F_{\mathrm{IA}}, F_{\mathrm{IIA}}, \hat{F}_{\mathrm{IA}}$ are indicated, where $\hat{F}_{\mathrm{IA}}$ is defined by the following equations [22–24].

$$\left.\begin{aligned} &\hat{K}_{\mathrm{IA}} = \left(\frac{3}{4}\cos\frac{\theta}{2} + \frac{1}{4}\cos\frac{3}{2}\theta\right)K_{\mathrm{IA}} + \left(\frac{3}{4}\sin\frac{\theta}{2} + \frac{3}{4}\sin\frac{3}{2}\theta\right)K_{\mathrm{IIA}}, \\ &\theta = -\varphi, \hat{F}_{\mathrm{IA}} = \hat{K}_{\mathrm{I}}/(\sigma_z^{\infty}\sqrt{\pi b\cos\varphi}) \text{ in Fig. 10(a)}, \\ &\theta = \varphi, \hat{F}_{\mathrm{IA}} = \hat{K}_{\mathrm{I}}/(\sigma_y^{\infty}\sqrt{\pi b\sin\varphi}) \text{ in Fig. 10(b)} \end{aligned}\right\} \tag{8}$$

In Eq. (8), K_{IA} and K_{IIA} are mode I and mode II stress intensity factors at A of an inclined crack (see Fig. 1). Tables 4–7 indicate the results for the projected cracks, F_{IA}^{0} and F_{IA}^{90}, whose inclination angles are $\varphi = 0°$, $\varphi = 90°$. Here, the projected crack in the xy^* plane has dimensions $(a, b\cos\varphi)$, and the projected crack

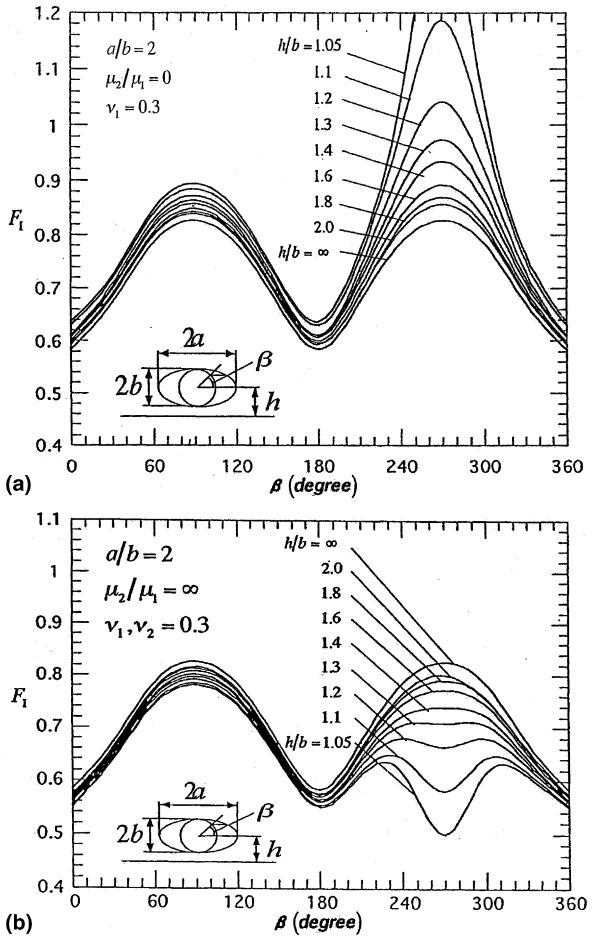

Fig. 9. Variation of $F_{\mathrm{I}}(\beta)$ in Fig. 4 with $a/b = 2$, ν_1, $\nu_2 = 0.3$: (a) when $\mu_2/\mu_1 = 0$, (b) when $\mu_2/\mu_1 = \infty$.

in the xz^* plane has dimensions $(a, b\sin\varphi)$. Then the following dimensionless factors are indicated and compared with $\hat{F}_{\mathrm{IA}}$.

$$\left.\begin{aligned} F^{0}_{\mathrm{IA}} &= K_{\mathrm{IA}}/(\sigma^{\infty}_{z}\sqrt{\pi b\cos\varphi}) \\ F^{90}_{\mathrm{IA}} &= K_{\mathrm{IA}}/(\sigma^{\infty}_{y}\sqrt{\pi b\sin\varphi}) \end{aligned}\right\} \tag{9}$$

In Figs. 11 and 12, $\hat{F}_{\mathrm{IA}}$ vs. h/b relations are shown when $\mu_2/\mu_1 = 0, \infty$. The difference between $\hat{F}_{\mathrm{IA}}$ and $\hat{F}^{0}_{\mathrm{IA}}$ (or F^{90}_{IA}) becomes large as the crack approaches the interface. However, in the range $1.05 \leqslant h/b < 1.2$, the difference is within 24% for remote tension parallel to the interface, and the difference is within 15% for remote tension vertical to the interface. In the range $h/b \geqslant 1.2$, the difference is within 15% for remote tension parallel to the interface, and the difference is within 11% for remote tension vertical to the interface. For the case of slightly inclined cracks when $\varphi = 15°, 75$, the difference is small even when $h/b = 1.05$. It may be concluded that the intensity of the stress singularity vertical to the tensile direction for an inclined crack can be estimated as the projected crack except for the case of very close to the interface.

4. Conclusion

The structural strength of composite materials is controlled to a considerable extent by the size, shape, orientation, and distribution of the flaws and imperfections, which exist in the material. Usually these flaws and

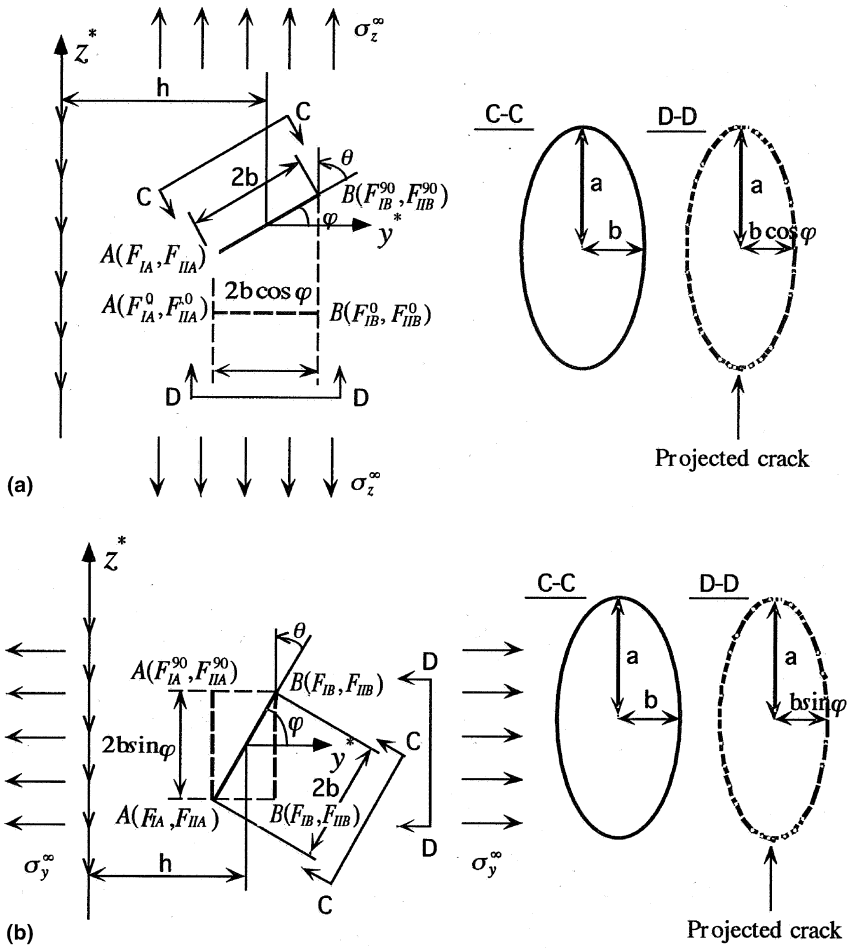

Fig. 10. Crack projected on the plane perpendicular to the tensile stress: (a) crack vertical to a bimaterial interface. (b) crack parallel to a bimaterial interface.

imperfections exhibit themselves in the form of entrapped gas or weak impurities on the interface, ruptured bonds, cracks, inclusions, and geometric singularities arising from the particular shape of the constituent materials. In this study, therefore, an inclined elliptical crack near a bimaterial interface was considered. The stress intensity factors were calculated systematically with varying the aspect ratio of crack, elastic modulus ratio, and distance from the interface. The conclusion can be made as follows.

(1) The results show that the present method has convergence to the fourth digit when $a/b = 1, 2, \infty$ and $h/b \geqslant 1.05$ in Fig. 1 (see Tables 1 and 2). The present method gives smooth variations of stress intensity factors along the crack front because unknown body force densities are approximated by using fundamental densities and polynomials. The results of Lee et al. [7] have about 16% deviations at most (when $\beta = -90°$ in Fig. 3(b)).

(2) The results for the vertical crack show that $\sqrt{\text{area}}$ parameter F_1^* may be useful for engineering applications because the value of F_1^* is insensitive to a/b. In other words, different shaped cracks have nearly the same values of F_1^* (see Table 3, Figs. 5 and 6).

(3) It may be concluded that the stress intensity factors of an inclined crack $\hat{F}_{\mathrm{IA}}$ can be evaluated from the results of the projected crack F_{IA}^0 (or F_{IA}^{90}). In the range of $1.05 \leqslant h/b < 1.2'$ the difference is within 24%, and in the range of $h/b \geqslant 1.2'$ the difference is within 15% involving the case of inclination angle $\varphi = 45°$ (see Table 4, Figs. 11 and 12).

Table 4
Dimensionless stress intensity factors F_{IA}, F_{IIA}, $\hat{F}_{IA}$, F^0_{IA}, $\hat{F}_{IA}/F^0_{IA}$ at $\beta = 3\pi/2$ when $\varphi = 15°$, ν_1, $\nu_2 = 0.3$ in Fig. 1 when $\sigma^\infty_z = \sigma$, $\sigma^\infty_y = 0$ (see Fig. 10(a))

h/b	a/b	F_{IA}		F_{IIA}		$\hat{F}_{IA}$		F^0_{IA}		$\hat{F}_{IA}/F^0_{IA}$	
		$\mu_2/\mu_1 = 0$	$\mu_2/\mu_1 = \infty$	$\mu_2/\mu_1 = 0$	$\mu_2/\mu_1 = \infty$	$\mu_2/\mu_1 = 0$	$\mu_2/\mu_1 = \infty$	$\mu_2/\mu_1 = 0$	$\mu_2/\mu_1 = \infty$	$\mu_2/\mu_1 = 0$	$\mu_2/\mu_1 = \infty$
1.05	1	0.8151	0.3190	0.2556	0.0926	0.9084	0.3526	0.7952	0.4012	1.1495	0.8789
	2	1.2354	0.4059	0.3021	0.0972	1.3433	0.4406	1.2172	0.5102	1.1036	0.8636
	∞	1.8611	0.5056	0.4231	0.1075	2.0112	0.5435	1.7534	0.6146	1.1470	0.8843
1.1	1	0.7404	0.3599	0.2301	0.1031	0.8243	0.3973	0.7751	0.4456	1.0635	0.8916
	2	1.1182	0.4624	0.2942	0.1129	1.2240	0.5027	1.1293	0.5634	1.0839	0.8922
	∞	1.6156	0.5896	0.3831	0.1212	1.7521	0.6321	1.6181	0.6752	1.0828	0.9362
1.2	1	0.6780	0.4293	0.2251	0.1135	0.7605	0.4701	0.7362	0.5071	1.0330	0.9270
	2	0.9685	0.5398	0.2854	0.1349	1.0722	0.5881	1.0262	0.6351	1.0448	0.9260
	∞	1.3690	0.6781	0.3632	0.1468	1.4997	0.7299	1.4436	0.7557	1.0389	0.9659
1.4	1	0.6347	0.5240	0.2019	0.1387	0.7084	0.5739	0.6885	0.5919	1.0289	0.9696
	2	0.8741	0.6350	0.2494	0.1408	0.9644	0.6848	0.9301	0.7254	1.0369	0.9440
	∞	1.1777	0.7675	0.3047	0.1916	1.2871	0.8361	1.2444	0.8417	1.0343	0.9933
1.6	1	0.6179	0.5542	0.1943	0.1626	0.6888	0.6132	0.6703	0.6124	1.0276	1.0013
	2	0.8347	0.6831	0.2365	0.1817	0.9203	0.7485	0.8893	0.7647	1.0349	0.9788
	∞	1.0970	0.8141	0.2823	0.2124	1.1983	0.8904	1.1675	0.8847	1.0264	1.0264
2.0	1	0.6046	0.5772	0.1894	0.1785	0.6737	0.6423	0.6585	0.6264	1.0231	1.0254
	2	0.8010	0.7243	0.2277	0.2034	0.8835	0.7979	0.8588	0.7879	1.0288	1.0127
	∞	1.0244	0.8621	0.2646	0.2309	1.1114	0.9453	1.0833	0.9339	1.0259	1.0122
∞	1	0.5940	0.5940	0.1872	0.1872	0.6623	0.6623	0.6476	0.6476	1.0227	1.0227
	2	0.7704	0.7704	0.2239	0.2239	0.8516	0.8516	0.8331	0.8331	1.0222	1.0222
	∞	0.9330	0.9330	0.2500	0.2500	1.0231	1.0231	1.0000	1.0000	1.0231	1.0231

Table 5
Dimensionless stress intensity factors F_{IA}, F_{IIA}, $\hat{F}_{IA}$, F^0_{IA}, $\hat{F}_{IA}/F^0_{IA}$ at $\beta = 3\pi/2$ when $\varphi = 45°$, ν_1, $\nu_2 = 0.3$ in Fig. 1 when $\sigma^\infty_z = \sigma$, $\sigma^\infty_y = 0$ (see Fig. 10(a))

h/b	a/b	F_{IA}		F_{IIA}		$\hat{F}_{IA}$		F^0_{IA}		$\hat{F}_{IA}/F^0_{IA}$	
		$\mu_2/\mu_1 = 0$	$\mu_2/\mu_1 = \infty$	$\mu_2/\mu_1 = 0$	$\mu_2/\mu_1 = \infty$	$\mu_2/\mu_1 = 0$	$\mu_2/\mu_1 = \infty$	$\mu_2/\mu_1 = 0$	$\mu_2/\mu_1 = \infty$	$\mu_2/\mu_1 = 0$	$\mu_2/\mu_1 = \infty$
1.05	1	0.4139	0.2533	0.5156	0.2642	0.9890	0.5454	0.8631	0.6095	1.1459	0.8948
	2	0.6436	0.2751	0.7149	0.2801	1.4367	0.5844	1.1564	0.6806	1.2423	0.8587
	∞	1.1662	0.2881	0.8749	0.2917	2.1132	0.6101	1.7002	0.7214	1.2429	0.8457
1.1	1	0.3471	0.2768	0.5012	0.2787	0.9096	0.5689	0.8224	0.6287	1.1060	0.9049
	2	0.5666	0.2903	0.6608	0.2960	1.3014	0.6172	1.0923	0.7056	1.1914	0.8747
	∞	0.9419	0.3085	0.8349	0.3106	1.8562	0.6512	1.5856	0.7472	1.1707	0.8715
1.2	1	0.3019	0.2855	0.4836	0.2916	0.8467	0.6075	0.7825	0.6584	1.0820	0.9227
	2	0.4747	0.3025	0.6316	0.3374	1.1812	0.6769	1.0305	0.7408	1.1462	0.9137
	∞	0.7004	0.3353	0.7813	0.3602	1.5673	0.7342	1.3936	0.7961	1.1246	0.9222
1.4	1	0.3134	0.2978	0.4335	0.3371	0.7991	0.6721	0.7636	0.6890	1.0465	0.9755
	2	0.4564	0.3590	0.5475	0.3728	1.0660	0.7711	0.9516	0.7860	1.1202	0.9810
	∞	0.6296	0.3761	0.6650	0.4112	1.3654	0.8319	1.2444	0.8407	1.0972	0.9895
1.6	1	0.3181	0.3034	0.4124	0.3512	0.7789	0.6938	0.7529	0.7044	1.0345	0.9850
	2	0.4463	0.3822	0.5146	0.4075	1.0182	0.8333	0.9177	0.8168	1.1095	1.0202
	∞	0.5982	0.4043	0.6141	0.4325	1.2766	0.8832	1.1675	0.8739	1.0934	1.0106
2.0	1	0.3210	0.3104	0.3931	0.3615	0.7591	0.7124	0.7488	0.7247	1.0138	0.9830
	2	0.4354	0.3927	0.4832	0.4148	0.9704	0.8516	0.9032	0.8440	1.0744	1.0090
	∞	0.5662	0.4397	0.5657	0.4530	1.1902	0.9402	1.0913	0.9268	1.0906	1.0145
∞	1	0.3183	0.3183	0.3745	0.3745	0.7349	0.7349	0.7404	0.7404	0.9926	0.9926
	2	0.4129	0.4129	0.4478	0.4478	0.9090	0.9090	0.8892	0.8892	1.0223	1.0223
	∞	0.5000	0.5000	0.5000	0.5000	1.0516	1.0516	1.0000	1.0000	1.0516	1.0516

Table 6
Dimensionless stress intensity factors F_{IA}, F_{IIA}, $\hat{F}_{IA}$, F^0_{IA}, $\hat{F}_{IA}/F^{90}_{IA}$ at $\beta = 3\pi/2$ when $\varphi = 45°$, ν_1, $\nu_2 = 0.3$ in Fig. 1 when $\sigma^\infty_z = 0$, $\sigma^\infty_y = \sigma$ (see Fig. 10(b))

h/b	a/b	F_{IA}		F_{IIA}		$\hat{F}_{IA}$		F^{90}_{IA}		$\hat{F}_{IA}/F^{90}_{IA}$	
		$\mu_2/\mu_1 = 0$	$\mu_2/\mu_1 = \infty$	$\mu_2/\mu_1 = 0$	$\mu_2/\mu_1 = \infty$	$\mu_2/\mu_1 = 0$	$\mu_2/\mu_1 = \infty$	$\mu_2/\mu_1 = 0$	$\mu_2/\mu_1 = \infty$	$\mu_2/\mu_1 = 0$	$\mu_2/\mu_1 = \infty$
1.05	1	0.4139	0.4024	−0.5156	−0.1442	0.9890	0.5454	1.1522	0.5821	0.8584	0.9370
	2	0.6436	0.4703	−0.7149	−0.1230	1.4367	0.5844	1.6713	0.6371	0.8596	0.9173
	∞	1.1662	0.4081	−0.8749	−0.1951	2.1132	0.6101	2.4013	0.6814	0.8800	0.8954
1.1	1	0.3471	0.3815	−0.5012	−0.1812	0.9096	0.5689	1.0226	0.6031	0.8894	0.9433
	2	0.5666	0.4601	−0.6608	−0.1594	1.3014	0.6172	1.5027	0.6653	0.8660	0.9277
	∞	0.9419	0.4209	−0.8349	−0.2201	1.8562	0.6512	2.1165	0.7162	0.8770	0.9092
1.2	1	0.3019	0.3780	−0.4836	−0.2171	0.8467	0.6075	0.9094	0.6301	0.9311	0.9641
	2	0.4747	0.4557	−0.6316	−0.2142	1.1812	0.6769	1.3024	0.7024	0.9069	0.9637
	∞	0.7004	0.4227	−0.7813	−0.2899	1.5673	0.7342	1.7091	0.7771	0.9170	0.9448
1.4	1	0.3134	0.3521	−0.4335	−0.2934	0.7991	0.6721	0.8204	0.6569	0.9740	1.0231
	2	0.4564	0.4418	−0.5475	−0.3061	1.0660	0.7711	1.1097	0.7597	0.9606	1.0150
	∞	0.6296	0.4406	−0.6650	−0.3593	1.3654	0.8319	1.4385	0.8323	0.9492	0.9995
1.6	1	0.3181	0.3361	−0.4124	−0.3249	0.7789	0.6938	0.7634	0.6569	1.0203	1.0562
	2	0.4463	0.4267	−0.5146	−0.3536	1.0182	0.8333	1.0097	0.7597	1.0084	1.0969
	∞	0.5982	0.4492	−0.6141	−0.3964	1.2766	0.8832	1.2995	0.8323	0.9824	1.0612
2.0	1	0.3210	0.3228	−0.3931	−0.3516	0.7591	0.7124	0.7404	0.6762	1.0253	1.0535
	2	0.4354	0.4121	−0.4832	−0.3991	0.9704	0.8516	0.9397	0.7997	1.0327	1.0649
	∞	0.5662	0.4603	−0.5657	−0.4364	1.1902	0.9402	1.1629	0.8731	1.0235	1.0768
∞	1	0.3183	0.3183	−0.3745	−0.3745	0.7349	0.7349	0.7404	0.7404	0.9926	0.9926
	2	0.4129	0.4129	−0.4478	−0.4478	0.9090	0.9090	0.8892	0.8892	1.0223	1.0223
	∞	0.5000	0.5000	−0.5000	−0.5000	1.0516	1.0516	1.0000	1.0000	1.0516	1.0516

Table 7
Dimensionless stress intensity factors F_{IA}, F_{IIA}, $\hat{F}_{IA}$, F^0_{IA}, $\hat{F}_{IA}/F^{90}_{IA}$ at $\beta = 3\pi/2$ when $\varphi = 75°$, ν_1, $\nu_2 = 0.3$ in Fig. 1 when $\sigma^\infty_z = 0$, $\sigma^\infty_y = \sigma$ (see Fig. 10(b))

h/b	a/b	F_{IA}		F_{IIA}		$\hat{F}_{IA}$		F^{90}_{IA}		$\hat{F}_{IA}/F^{90}_{IA}$	
		$\mu_2/\mu_1 = 0$	$\mu_2/\mu_1 = \infty$	$\mu_2/\mu_1 = 0$	$\mu_2/\mu_1 = \infty$	$\mu_2/\mu_1 = 0$	$\mu_2/\mu_1 = \infty$	$\mu_2/\mu_1 = 0$	$\mu_2/\mu_1 = \infty$	$\mu_2/\mu_1 = 0$	$\mu_2/\mu_1 = \infty$
1.05	1	0.8464	0.2697	−0.2486	−0.0834	0.9366	0.3001	1.0998	0.3246	0.8516	0.9245
	2	1.3979	0.3771	−0.3248	−0.0873	1.5134	0.4081	1.6822	0.4484	0.8997	0.9101
	∞	1.9457	0.4695	−0.4386	−0.1087	2.1011	0.5081	2.4098	0.5642	0.8719	0.9006
1.1	1	0.7605	0.3357	−0.2286	−0.0943	0.8436	0.3698	0.9413	0.4127	0.8962	0.8961
	2	1.1734	0.4512	−0.3021	−0.1098	1.2818	0.4904	1.4158	0.5467	0.9054	0.8970
	∞	1.5966	0.5737	−0.3842	−0.1196	1.7336	0.6157	1.9315	0.6801	0.8975	0.9053
1.2	1	0.6891	0.4196	−0.2144	−0.1068	0.7673	0.4579	0.8154	0.4871	0.9410	0.9401
	2	1.0174	0.5471	−0.2848	−0.1188	1.1204	0.5890	1.2070	0.6268	0.9283	0.9397
	∞	1.3155	0.6828	−0.3527	−0.1374	1.4426	0.7309	1.5313	0.7756	0.9421	0.9424
1.4	1	0.6612	0.5211	−0.2042	−0.1383	0.7356	0.5709	0.7676	0.5793	0.9583	0.9855
	2	0.9512	0.6296	−0.2624	−0.1210	1.0460	0.6800	1.0931	0.6895	0.9569	0.9862
	∞	1.2432	0.7706	−0.2941	−0.1861	1.3479	0.8370	1.3942	0.8447	0.9668	0.9909
1.6	1	0.6431	0.5609	−0.1983	−0.1544	0.7154	0.6166	0.7354	0.6121	0.9728	1.0074
	2	0.9066	0.6765	−0.2490	−0.1403	0.9965	0.7358	1.0153	0.7266	0.9815	1.0127
	∞	1.1823	0.8118	−0.2794	−0.2054	1.2818	0.8854	1.3040	0.8751	0.9830	1.0118
2.0	1	0.6224	0.5840	−0.1923	−0.1569	0.6925	0.6405	0.6775	0.6232	1.0221	1.0278
	2	0.8528	0.7229	−0.2353	−0.1645	0.9378	0.7814	0.9259	0.7630	1.0129	1.0238
	∞	1.1049	0.8440	−0.2613	−0.2191	1.1979	0.9227	1.1958	0.9076	1.0018	1.0166
∞	1	0.5940	0.5940	−0.1872	−0.1872	0.6623	0.6623	0.6476	0.6476	1.0227	1.0227
	2	0.7704	0.7704	−0.2239	−0.2239	0.8516	0.8516	0.8331	0.8331	1.0222	1.0222
	∞	0.9330	0.9330	−0.2500	−0.2500	1.0231	1.0231	1.0000	1.0000	1.0231	1.0231

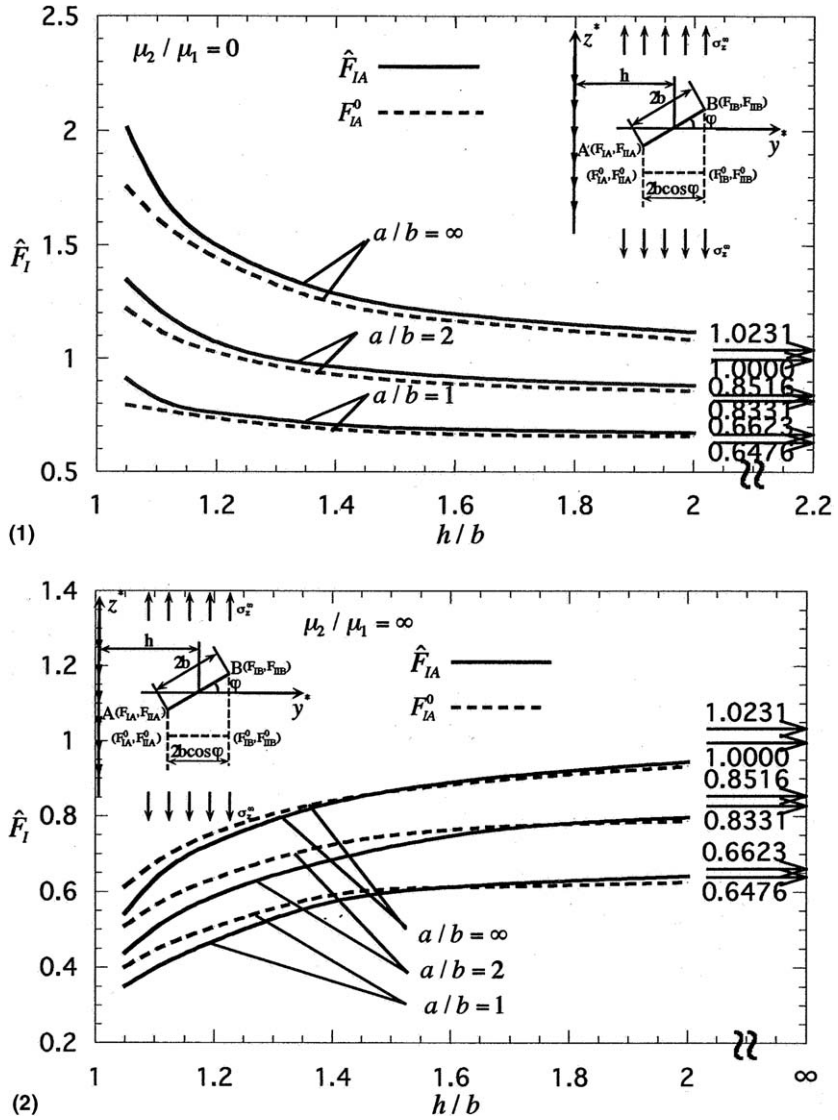

Fig. 11a. $\hat{F}_{IA}$, F^0_{IA} vs. h/b in Fig. 1 with $\varphi = 15°$, ν_1, $\nu_2 = 0.3$: (1) when $\mu_2/\mu_1 = 0$, (2) when $\mu_2/\mu_1 = \infty$.

Acknowledgements

This research has been partly supported by JSPS postdoctoral fellowship and Kyushu Institute of Technology fellowship for foreign researchers. The authors wish to express their thanks to the members of their group, especially Mr. S. Fujimoto, Mr. Y. Shimomoto, Mr. S. Egawa, and Mr. M. Tsuyunaru, who carried out much of the constructional work.

Appendix A. Stress and displacement fields due to a point force in a bimaterial

Consider a bimaterial whose interface is in x_1x_2 plane as shown in Fig. A.1. Then, the displacement and stress fields due to a point force P, which is vertical to the interface, can be expressed as the following equations [25,26].

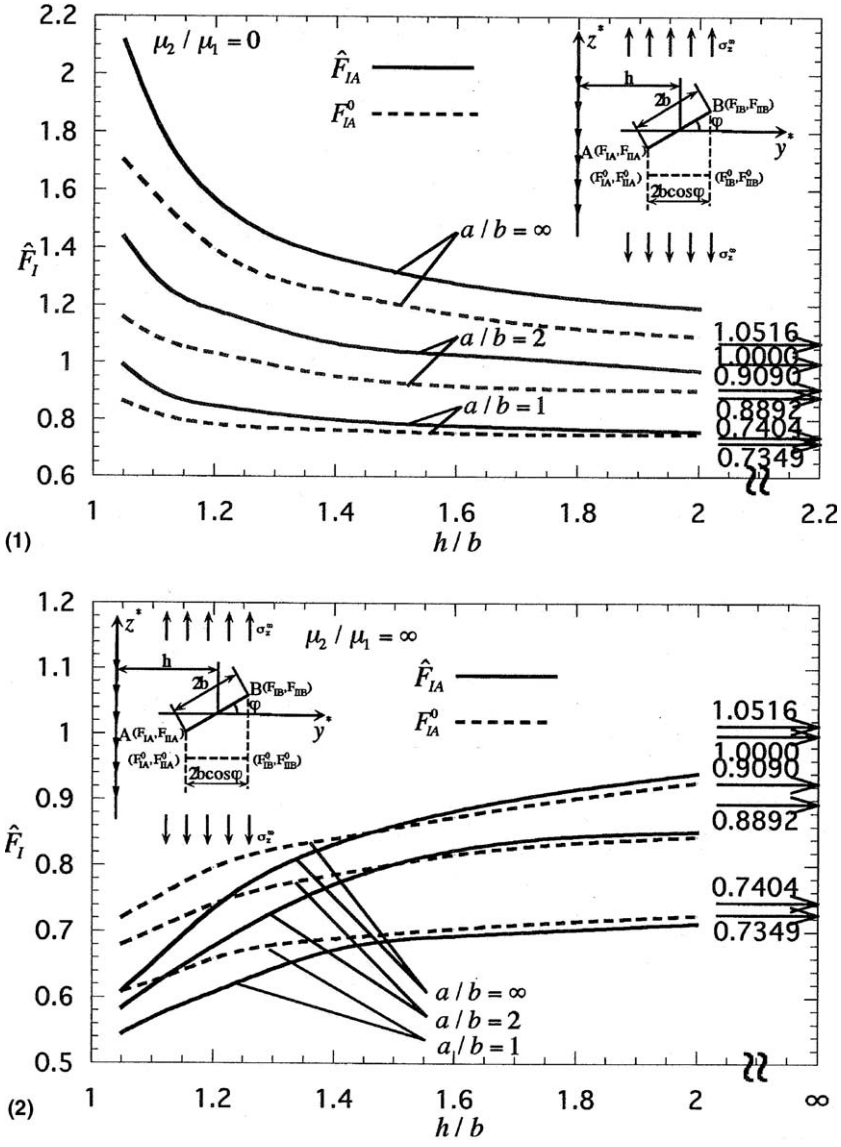

Fig. 11b. $\hat{F}_{\mathrm{IA}}$, F^0_{IA} vs. h/b in Fig. 1 with $\varphi = 45°$, ν_1, $\nu_2 = 0.3$: (1) when $\mu_2/\mu_1 = 0$, (2) when $\mu_2/\mu_1 = \infty$.

For space 1

$$u^p_{11} = \frac{Px_1}{4\mu_1\pi(\kappa_1+1)}\left\{\frac{(x_3-c)}{r_1^3}+\frac{A\kappa_1(x_3-c)}{r_2^3}+\frac{6Ax_3c(x_3-c)}{r_2^5}-\frac{TS(\kappa_1+1)}{r_2(r_2+x_3+c)}\right\}$$

$$u^p_{21} = \frac{Px_2}{4\mu_1\pi(\kappa_1+1)}\left\{\frac{(x_3-c)}{r_1^3}+\frac{A\kappa_1(x_3-c)}{r_2^3}+\frac{6Ax_3c(x_3-c)}{r_2^5}-\frac{TS(\kappa_1+1)}{r_2(r_2+x_3+c)}\right\}$$

$$u^p_{31} = \frac{P}{4\mu_1\pi(\kappa_1+1)}\left\{\frac{\kappa_1}{r_1}+\frac{(x_3-c)^2}{r_1^3}+\frac{A\kappa_1^2-TS(\kappa_1-1)}{r_2}+\frac{A\kappa_1(x_3+c)^2-2Ax_3c}{r_2^3}+\frac{6Ax_3c(x_3+c)^2}{r_2^5}\right\} \qquad \text{(A.1)}$$

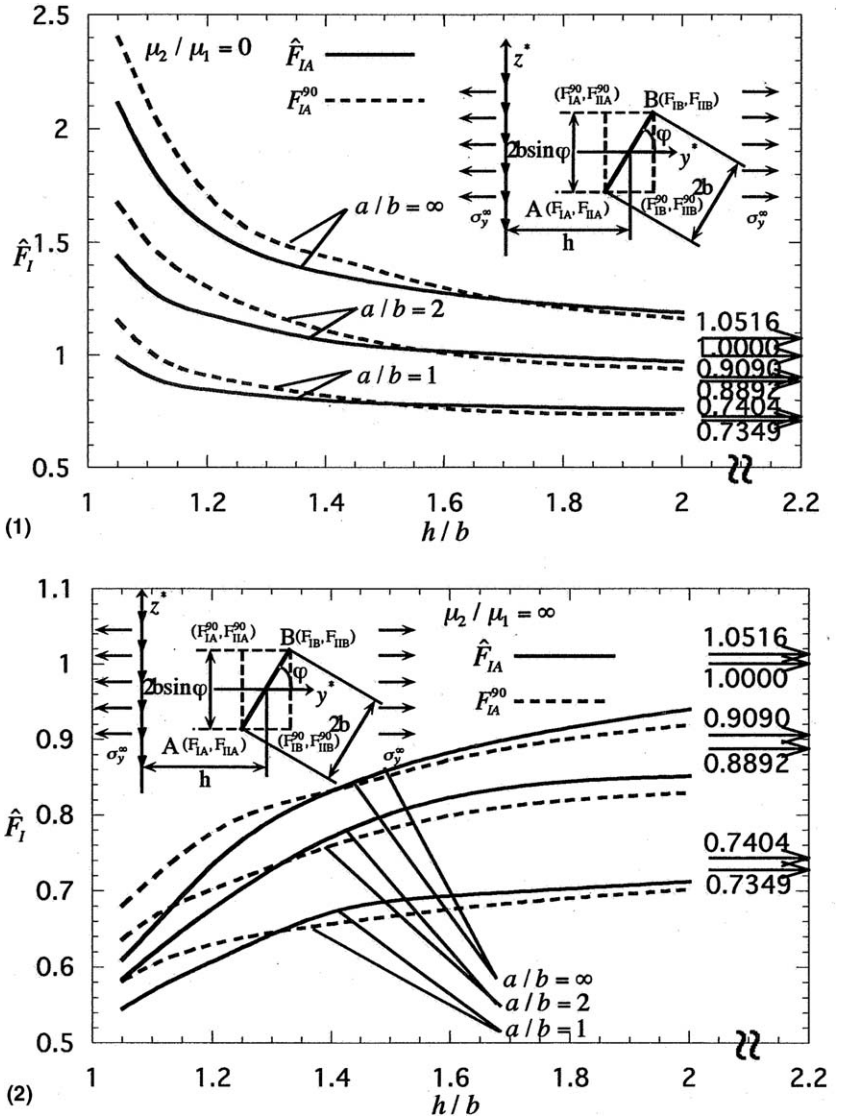

Fig. 12a. $\hat{F}_{\mathrm{IA}}$, F_{IA}^{90} vs. h/b in Fig. 1 with $\varphi = 45°$, ν_1, $\nu_2 = 0.3$: (1) when $\mu_2/\mu_1 = 0$, (2) when $\mu_2/\mu_1 = \infty$.

$$\sigma_{111}^{p} = \frac{P}{2\pi(\kappa_1+1)}\left\{\frac{(\kappa_1-1)(x_3-c)}{2r_1^3} - \frac{3x_1^2(x_3-c)}{r_1^5} + \frac{A(\kappa_1-3)(\kappa_1-1)(x_3+c)}{2r_2^3} + \frac{3A(\kappa_1-1)(x_3-c)}{2r_2^3}\right.$$

$$+ \frac{3A(\kappa_1-1)c(x_3+c)^2 - 6Ac^2(x_3+c)}{r_2^5} - \frac{3A\kappa_1 x_1^2(x_3-c)}{r_2^5} - \frac{30Ax_3cx_1^2(x_3+c)}{r_2^7}$$

$$\left. - TS(\kappa_1+1)\left[\frac{1}{r_2(r_2+x_3+c)} - \frac{x_1^2(2r_2+x_3+c)}{r_2^3(r_2+x_3+c)^2}\right]\right\}$$

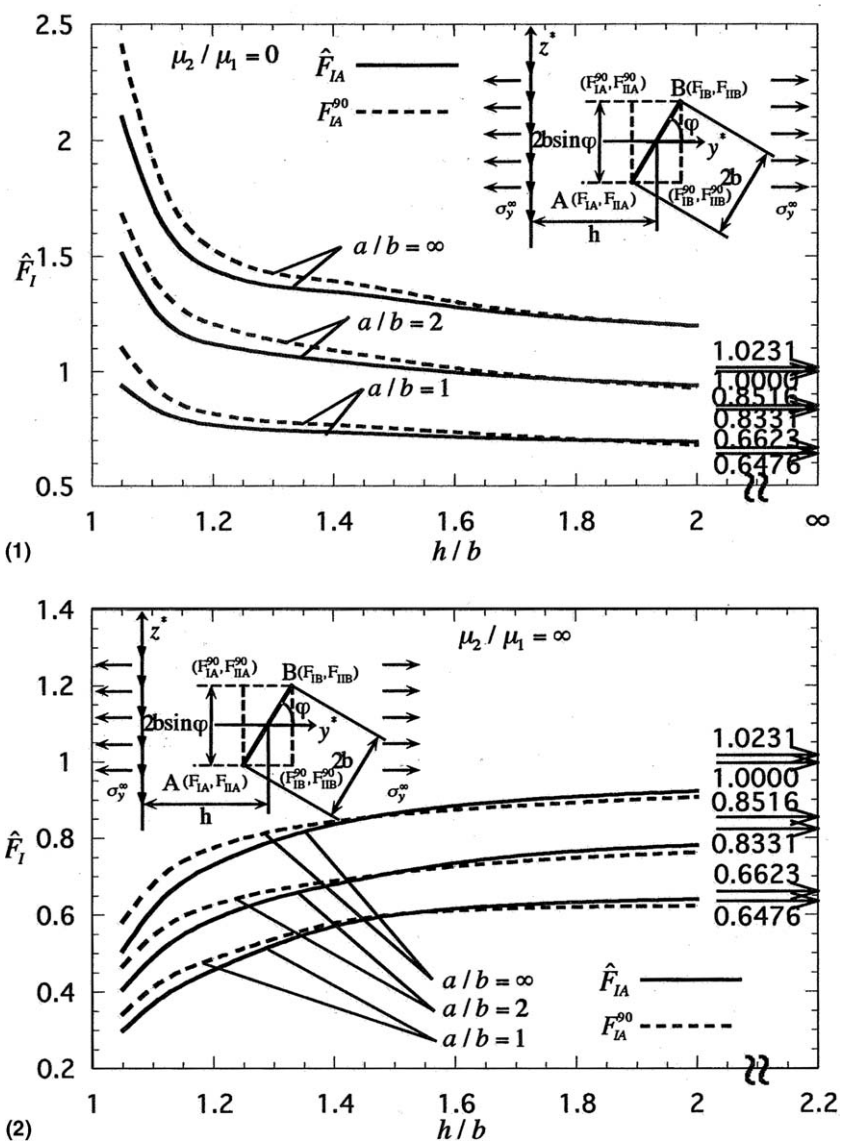

Fig. 12b. $\hat{F}_{IA}$, F_{IA}^{90} vs. h/b in Fig. 1 with $\varphi = 75°$, ν_1, $\nu_2 = 0.3$: (1) when $\mu_2/\mu_1 = 0$, (2) when $\mu_2/\mu_1 = \infty$.

$$\sigma_{221}^{p} = \frac{P}{2\pi(\kappa_1+1)}\left\{\frac{(\kappa_1-1)(x_3-c)}{2r_1^3} - \frac{3x_2^2(x_3-c)}{r_1^5} + \frac{A(\kappa_1-3)(\kappa_1-1)(x_3+c)}{2r_2^3}\right.$$
$$+\frac{3A(\kappa_1-1)(x_3-c)}{2r_2^3} + \frac{3A(\kappa_1-1)c(x_3+c)^2 - 6Ac^2(x_3+c)}{r_2^5}$$
$$-\frac{3A\kappa_1 x_2^2(x_3-c)}{r_2^5} - \frac{30Ax_3cx_2^2(x_3+c)}{r_2^7}$$
$$\left.-TS(\kappa_1+1)\left[\frac{1}{r_2(r_2+x_3+c)} - \frac{x_2^2(2r_2+x_3+c)}{r_2^3(r_2+x_3+c)^2}\right]\right\}$$

$$\sigma^p_{331}=\frac{P}{2\pi(\kappa_1+1)}\left\{\frac{(1-\kappa_1)(x_3-c)}{2r_1^3}-\frac{3(x_3-c)^3}{r_1^5}+\frac{[2TS(\kappa_1+1)-A(\kappa_1^2-3)](x_3+c)}{2r_2^3}\right.$$
$$+\frac{A(\kappa_1-3)(x_3-c)-4Ac}{2r_2^3}-\frac{3A\kappa_1x_3(x_3+c)^2-3Ac(x_3+c)(5x_3+c)}{r_2^5}$$
$$\left.-\frac{30Ax_3c(x_3+c)^3}{r_2^7}\right\}$$
$$\sigma^p_{121}=\frac{Px_1x_2}{2\pi(\kappa_1+1)}\left\{\frac{3(x_3-c)}{r_1^5}-\frac{3A\kappa_1(x_3-c)}{r_1^5}-\frac{30Ax_3c(x_3+c)}{r_2^7}\right.$$
$$\left.+\frac{TS(\kappa_1+1)(2r_2+x_3+c)}{r_2^3(r_2+x_3+c)^2}\right\}$$
$$\sigma^p_{131}=\frac{Px_1}{2\pi(\kappa_1+1)}\left\{\frac{(1-\kappa_1)}{2r_1^3}-\frac{3(x_3-c)^2}{r_1^5}+\frac{A\kappa_1-A\kappa_1^2+2TS(\kappa_1+1)}{2r_2^3}\right.$$
$$\left.-\frac{3A\kappa_1x_3(x_3-c)-3Ac(3x_3+c)}{r_2^5}-\frac{30Ax_3c(x_3+c)^2}{r_2^7}\right\}$$
$$\sigma^p_{231}=\frac{Px_2}{2\pi(\kappa_1+1)}\left\{\frac{(1-\kappa_1)}{2r_1^3}-\frac{3(x_3-c)^2}{r_1^5}+\frac{A\kappa_1-A\kappa_1^2+2TS(\kappa_1+1)}{2r_2^3}\right.$$
$$\left.-\frac{3A\kappa_1x_3(x_3-c)-3Ac(3x_3+c)}{r_2^5}-\frac{30Ax_3c(x_3+c)^2}{r_2^7}\right\} \tag{A.2}$$

For Space 2

$$u^p_{12}=\frac{\Gamma Px_1}{4\mu_2\pi(\kappa_2+1)}\left\{\frac{(1-\bar{A})(x_3-c)-\bar{T}S(\kappa_2+1)x_3}{r_1^3}-\frac{TS(\kappa_2+1)}{r_1(r_1+x_3+c)}\right\}$$
$$u^p_{22}=\frac{\Gamma Px_2}{4\mu_2\pi(\kappa_2+1)}\left\{\frac{(1-\bar{A})(x_3-c)-\bar{T}S(\kappa_2+1)x_3}{r_1^3}-\frac{TS(\kappa_2+1)}{r_1(r_1+x_3+c)}\right\}$$
$$u^p_{32}=\frac{\Gamma P}{4\mu_2\pi(\kappa_2+1)}\left\{\frac{(1-\bar{A})\kappa_1-TS(\kappa_2+1)}{r_1}+\frac{(1-\bar{A})(x_3-c)^2-\bar{T}S(\kappa_2+1)x_3(x_3-c)}{r_1^3}\right\} \tag{A.3}$$
$$\sigma^p_{112}=\frac{\Gamma P}{2\pi(\kappa_2+1)}\left\{\frac{[(\kappa_2-3)(1-\bar{B})+2(1-\bar{A})](x_3-c)-2\bar{T}S(\kappa_2+1)x_3}{2r_1^3}.\right.$$
$$+\frac{3x_1^2[\bar{T}S(\kappa_2+1)x_3-(1-\bar{A})(x_3-c)]}{r_1^5}$$
$$\left.-TS(\kappa_2+1)\left[\frac{1}{r_1(r_1-x_3+c)}-\frac{x_1^2(2r_1-x_3+c)}{r_1^3(r_1+x_3+c)^2}\right]\right\}$$
$$\sigma^p_{222}=\frac{\Gamma P}{2\pi(\kappa_2+1)}\left\{\frac{[(\kappa_2-3)(1-\bar{B})+2(1-\bar{A})](x_3-c)-2\bar{T}S(\kappa_2+1)x_3}{2r_1^3}.\right.$$
$$+\frac{3x_2^2[\bar{T}S(\kappa_2+1)x_3-(1-\bar{A})(x_3-c)]}{r_1^5}$$
$$\left.-TS(\kappa_2+1)\left[\frac{1}{r_1(r_1-x_3+c)}-\frac{x_1^2(2r_1-x_3+c)}{r_1^3(r_1+x_3+c)^2}\right]\right\}$$

$$\sigma^{p}_{332}=\frac{\Gamma P}{2\pi(\kappa_2+1)}\left\{\frac{[(\kappa_2-3)(1-\bar{B})+2(2-\kappa_1)(1-\bar{A})+2(T-\bar{T})S(\kappa_2+1)](x_3-c)}{2r_1^3}\right.$$
$$\left.-\frac{\bar{T}S(\kappa_2+1)x_3}{r_1^3}+\frac{3(x_3-c)^2[\bar{T}S(\kappa_2+1)x_3-(1-\bar{A})(x_3-c)]}{r_1^5}\right\}$$

$$\sigma^{p}_{122}=\frac{\Gamma P x_1x_2}{2\pi(\kappa_2+1)}\left\{\frac{3\bar{T}S(\kappa_2+1)x_3-3(1-\bar{A})(x_3-c)}{r_1^5}+\frac{TS(\kappa_2+1)(2r_1-x_3+c)}{r_1^3(r_1+x_3+c)^2}\right\}$$

$$\sigma^{p}_{132}=\frac{\Gamma P x_1}{2\pi(\kappa_2+1)}\left\{\frac{\bar{T}S(\kappa_2+1)+(\kappa_1-1)(1-\bar{A})}{2r_1^3}\right.$$
$$\left.+\frac{3\bar{T}S(\kappa_2+1)x_3(x_3-c)-3(1-\bar{A})(x_3-c)^2}{r_1^5}\right\}$$

$$\sigma^{p}_{232}=\frac{\Gamma P x_2}{2\pi(\kappa_2+1)}\left\{\frac{\bar{T}S(\kappa_2+1)+(\kappa_1-1)(1-\bar{A})}{2r_1^3}+\frac{3\bar{T}S(\kappa_2+1)x_3(x_1-c)-3(1-\bar{A})(x_3-c)}{r_1^5}\right\} \tag{A.4}$$

On the other hand, the displacement and stress fields due to a point force Q, which is parallel to the interface, can be expressed as the following equations [25,26].

For space 1

$$u^{Q}_{11}=\frac{Q}{4\mu_1\pi(\kappa_1+1)}\left\{\frac{\kappa_1}{r_1}+\frac{x_1^2}{r_1^3}+\frac{2A\kappa_1^2-AS(\kappa_1^2-1)}{2r_2}+\frac{A\kappa_1x_1^2+2Ax_3c}{r_2^3}-\frac{6Ax_3cx_1^2}{r_2^5}\right.$$
$$\left.+\frac{S(\kappa_1+1)[A(\kappa_1-1)-2T]}{2}\left[\frac{1}{r_2+x_3+c}-\frac{x_1^2}{r_2(r_2+x_3+c)^2}\right]\right\}$$

$$u^{Q}_{21}=\frac{Qx_1x_2}{4\mu_1\pi(\kappa_1+1)}\left\{\frac{1}{r_1^3}+\frac{A\kappa_1}{r_2^3}-\frac{6Ax_3c(x_3+c)}{r_2^5}-\frac{S(\kappa_1+1)[A(\kappa_1-1)-2T]}{2r_2(r_2+x_2+c)^2}\right\}$$

$$u^{Q}_{31}=\frac{Qx_1}{4\mu_1\pi(\kappa_1+1)}\left\{\frac{(x_3-c)}{r_1^3}+\frac{A\kappa_1(x_3-c)}{r_2^3}+\frac{6Ax_3c(x_3+c)}{r_2^5}-\frac{TS(\kappa_1+1)}{r_2(r_2+x_3+c)^2}\right\} \tag{A.5}$$

$$\sigma^{Q}_{111}=\frac{Qx_1}{2\pi(\kappa_1+1)}\left\{\frac{(1-\kappa_1)}{2r_1^3}-\frac{3x_1^2}{r_1^5}+\frac{A(\kappa_1-1)[S(\kappa_1+1)-\kappa_1]}{2r_2^3}\right.$$
$$-\frac{3A\kappa_1x_1^2+3A(\kappa_1+3)c(x_3+c)-18Ac^2}{r_2^5}+\frac{30Ax_3cx_1^2}{r_2^7}$$
$$\left.-\frac{S(\kappa_1+1)[A(\kappa_1-1)-2T]}{2}\left[\frac{3}{r_2(r_2+x_3+c)^2}-\frac{x_1^2(3r_2+x_3+c)}{r_2^3(r_2+x_3+c)^3}\right]\right\}$$

$$\sigma^{Q}_{221}=\frac{Qx_1}{2\pi(\kappa_1+1)}\left\{\frac{(\kappa_1-1)}{2r_1^3}-\frac{3x_2^2}{r_1^5}+\frac{A\kappa_1(\kappa_1-1)}{2r_2^3}\right.$$
$$-\frac{3A\kappa_1x_2^2+3A(\kappa_1-1)c(x_3+c)-6Ac^2}{r_2^5}+\frac{30Ax_3cx_2^2}{r_2^7}$$
$$\left.-\frac{S(\kappa_1+1)[A(\kappa_1-1)-2T]}{2}\left[\frac{1}{r_2(r_2+x_3+c)^2}-\frac{x_2^2(3r_2+x_3+c)}{r_2^3(r_2+x_3+c)^3}\right]\right\}$$

$$
\begin{aligned}
\sigma_{331} &= \frac{Qx_1}{2\pi(\kappa_1+1)}\left\{\frac{(\kappa_1-1)}{2r_1^3}-\frac{3(x_3-c)^2}{r_1^5}+\frac{[A\kappa_1(\kappa_1-1)-2TS(\kappa_1+1)]}{2r_2^3}\right.\\
&\quad\left.-\frac{3A\kappa_1(x_3+c)^2-3A(\kappa_1-1)c(x_3+c)-6Ac^2}{r_2^5}+\frac{30Ax_3c(x_3+c)^2}{r_2^7}\right\}\\
\sigma^{Q}_{121} &= \frac{Qx_1}{2\pi(\kappa_1+1)}\left\{\frac{(1-\kappa_1)}{2r_1^3}-\frac{3x_1^2}{r_1^5}+\frac{AS(\kappa_1^2-1)-2A\kappa_1(\kappa_1-1)}{4r_2^3}-\frac{3A\kappa_1x_1^2+6Ax_3c}{r_2^5}\right.\\
&\quad\left.+\frac{30Ax_3cx_1^2}{r_2^7}-\frac{S(\kappa_1+1)[A(\kappa_1-1)-2T]}{2}\left[\frac{1}{r_2(r_2+x_3+c)^2}-\frac{x_1^2(3r_2+x_3+c)}{r_2^3(r_2+x_3+c)^3}\right]\right\}\\
\sigma^{Q}_{131} &= \frac{Q}{2\pi(\kappa_1+1)}\left\{\frac{(1-\kappa_1)(x_3-c)}{2r_1^3}-\frac{3x_1^2(x_3-c)}{r_1^5}\right.\\
&\quad+\frac{[AS(\kappa_1^2-1)-2A\kappa_1(\kappa_1-1)](x_3-c)-4A(\kappa_1-1)c}{4r_2^3}\\
&\quad-\frac{3A\kappa_1x_1^2(x_3+c)-3A(\kappa_1-1)cx_1^2+6Ax_3c(x_3+c)}{r_2^5}+\frac{30Ax_3cx_1^2(x_3+c)}{r_2^7}\\
&\quad\left.-\frac{S(\kappa_1+1)[A(\kappa_1-1)-4T]}{2}\left[\frac{1}{r_2(r_2+x_3+c)}-\frac{x_1^2(2r_2+x_3+c)}{r_2^3(r_2+x_3+c)^2}\right]\right\}\\
\sigma^{Q}_{231} &= \frac{Qx_1x_2}{2\pi(\kappa_1+1)}\left\{-\frac{3(x_3-c)}{r_1^5}-\frac{3A\kappa_1(x_3+c)-3A(\kappa_3-1)c}{r_2^5}+\frac{30Ax_3c(x_3+c)}{r_2^7}\right.\\
&\quad\left.+\frac{S(\kappa_1+1)[A(\kappa_1-1)-4T]2(r_2+x_3+c)}{4r_2^3(r_2+x_3+c)^2}\right\}
\end{aligned}
\tag{A.6}
$$

For space 2

$$
\begin{aligned}
u^{Q}_{12} &= \frac{\Gamma Q}{4\mu_2\pi(\kappa_2+1)}\left\{\frac{[2\kappa_1(1-\bar{A})-AS(\kappa_1-1)(\kappa_2+1)]}{2r_1}+\frac{(1-\bar{A})x_1^2}{r_1^3}\right.\\
&\quad-\bar{T}S(\kappa_2+1)x_3\left[\frac{1}{r_1(r_1-x_3+c)}-\frac{x_1^2(2r_1-x_3+c)}{r_1^3(r_1-x_3+c)^2}\right]\\
&\quad\left.+\frac{S(\kappa_2+1)[A(\kappa_1-1)-2T]}{2}\left[\frac{1}{r_1-x_3+c}-\frac{x_1^2}{r_1(r_1-x_3+c)^2}\right]\right\}\\
u^{Q}_{22} &= \frac{\Gamma Qx_1x_2}{4\mu_2\pi(\kappa_2+1)}\left\{\frac{(1-\bar{A})}{r_1^3}+\frac{\bar{T}S(\kappa_2+1)x_3(2r_1-x_3+c)}{r_1^3(r_1-x_3+c)^2}-\frac{S(\kappa_2+1)[A(\kappa_1-1)-2T]}{2r_1(r_1-x_3+c)^2}\right\}\\
u^{Q}_{32} &= \frac{\Gamma Qx_1}{4\mu_1\pi(\kappa_2+1)}\left\{\frac{(1-\bar{A})(x_3+c)-\bar{T}S(\kappa_2+1)x_3}{r_1^3}+\frac{TS(\kappa_2+1)}{r_1(r_1-x_3+c)}\right\}\\
\sigma^{Q}_{112} &= \frac{\Gamma Qx_1}{2\pi(\kappa_2+1)}\left\{\frac{(\kappa_2-3)(1-\bar{B})+2(2-\kappa_1)(1-\bar{A})+AS(\kappa_1-1)(\kappa_2+1)}{2r_1^3}\right.\\
&\quad-\frac{3(1-\bar{A})x_1^2}{r_1^5}-\frac{S(\kappa_2+1)[A(\kappa_1-1)-2T]}{2}\left[\frac{3}{r_1(r_1-x_3+c)^2}-\frac{x_1^2(3r_1-x_3+c)}{r_1^3(r_1-x_3+c)^3}\right]\\
&\quad\left.+\bar{T}S(\kappa_2+1)x_3\left[\frac{3(2r_1-x_3+c)}{r_1^3(r_1-x_3+c)^2}-\frac{3x_1^2(2r_1-x_3+c)}{r_1^5(r_1-x_3+c)^2}-\frac{2x_1^2}{r_1^3(r_1-x_3+c)^3}\right]\right\}
\end{aligned}
\tag{A.7}
$$

$$
\begin{aligned}
\sigma^{Q}_{222} &= \frac{\Gamma Q x_1}{2\pi(\kappa_2+1)}\left\{\frac{(\kappa_2-3)(1-\bar{B})+2(1-\bar{A})}{2r_1^3}-\frac{3(1-\bar{A})x_2^2}{r_1^5}\right.\\
&\quad -\frac{S(\kappa_2+1)[A(\kappa_1-1)-2T]}{2}\left[\frac{1}{r_1(r_1-x_3+c)^2}-\frac{x_2^2(3r_1-x_3+c)}{r_1^3(r_1-x_3+c)^3}\right]\\
&\quad \left.+\bar{T}S(\kappa_2+1)x_3\left[\frac{(2r_1-x_3+c)}{r_1^3(r_1-x_3+c)^2}-\frac{3x_2^2(2r_1-x_3+c)}{r_1^5(r_1-x_3+c)^2}-\frac{2x_2^2}{r_1^3(r_1-x_3+c)^3}\right]\right\}\\
\sigma^{Q}_{332} &= \frac{\Gamma Q x_1}{2\pi(\kappa_2+1)}\left\{\frac{(\kappa_2-3)(1-\bar{B})+2(1-\bar{A})+2(T-\bar{T})S(\kappa_2+1)}{2r_1^3}\right.\\
&\quad \left.+\frac{3\bar{T}S(\kappa_2+1)x_3(x_3+c)-3(1-\bar{A})(x_3+c)^2}{r_1^5}\right\}\\
\sigma^{Q}_{112} &= \frac{\Gamma Q x_2}{2\pi(\kappa_2+1)}\left\{\frac{2(1-\kappa_1)(1-\bar{A})+AS(\kappa_1-1)(\kappa_2+1)}{4r_1^3}-\frac{3(1-\bar{A})x_1^2}{r_1^5}\right.\\
&\quad -\frac{S(\kappa_2+1)[A(\kappa_1-1)-2T]}{2}\left[\frac{1}{r_1(r_1-x_3+c)^2}-\frac{x_1^2(3r_1-x_3+c)}{r_1^3(r_1-x_3+c)^3}\right]\\
&\quad \left.+\bar{T}S(\kappa_2+1)x_3\left[\frac{(2r_1-x_3+c)}{r_1^3(r_1-x_3+c)^2}-\frac{3x_1^2(2r_1-x_3+c)}{r_1^5(r_1-x_3+c)^2}-\frac{2x_1^2}{r_1^3(r_1-x_3+c)^3}\right]\right\}\\
\sigma^{Q}_{132} &= \frac{\Gamma Q}{2\pi(\kappa_2+1)}\left\{\frac{[2(1-\kappa_1)(1-\bar{A})+AS(\kappa_1-1)(\kappa_2+1)](x_3-c)-4\bar{T}S(\kappa_2+1)x_3}{4r_1^3}\right.\\
&\quad -\frac{3(1-\bar{A})x_1^2(x_3-c)-3\bar{T}S(\kappa_2+1)x_1^2x_3}{r_1^5}\\
&\quad \left.+\frac{S(\kappa_2+1)[A(\kappa_1-1)-2\bar{T}]}{4}\left[\frac{1}{r_1(r_1-x_3+c)}-\frac{x_1^2(2r_1-x_3+c)}{r_1^3(r_1-x_3+c)^2}\right]\right\}\\
\sigma^{Q}_{232} &= \frac{\Gamma Q x_1 x_2}{2\pi(\kappa_2+1)}\left\{\frac{3(1-\bar{A})(x_3-c)-3\bar{T}S(\kappa_2+1)x_3}{r_1^5}-\frac{S(\kappa_2+1)[A(\kappa_1-1)-2\bar{T}(2r_1-x_3+c)]}{4r_1^3(r_1-x_3+c)^2}\right\}
\end{aligned}
\tag{A.8}
$$

where

$$
\left.
\begin{aligned}
&\kappa_1 = 3-4\nu_1, \quad \kappa_2 = 3-4\nu_2\\
&\Gamma = \frac{\mu_2}{\mu_1}, \quad S = \frac{2}{1+\Gamma}\\
&A = \frac{1-\Gamma}{1+\Gamma\kappa_1}, \quad \bar{B} = \frac{\Gamma-1}{\kappa_2+\Gamma}\\
&T = \frac{1}{4}\left[\frac{\kappa_1-1}{1+\Gamma\kappa_1}-\frac{(\kappa_2-1)\Gamma}{\kappa_2+\Gamma}\right]\\
&r_2 = \sqrt{x_1^2+x_2^2+(x_3+c)^2}\\
&\bar{A} = \frac{\Gamma\kappa_1-\kappa_2}{1+\Gamma\kappa_1}, \quad B = \frac{\kappa_2-\Gamma\kappa_1}{\kappa_2+\Gamma}\\
&\bar{T} = \frac{1}{2}\left[\frac{\kappa_2-1}{\kappa_2+\Gamma}-\frac{(\kappa_1-1)\Gamma}{1+\Gamma\kappa_1}\right]
\end{aligned}
\right\}
\tag{A.9}
$$

Here μ_1, μ_2 are shear modulus, and ν_1, ν_2 are Poisson's ratio for space 1 and space 2 in Fig. A.1.

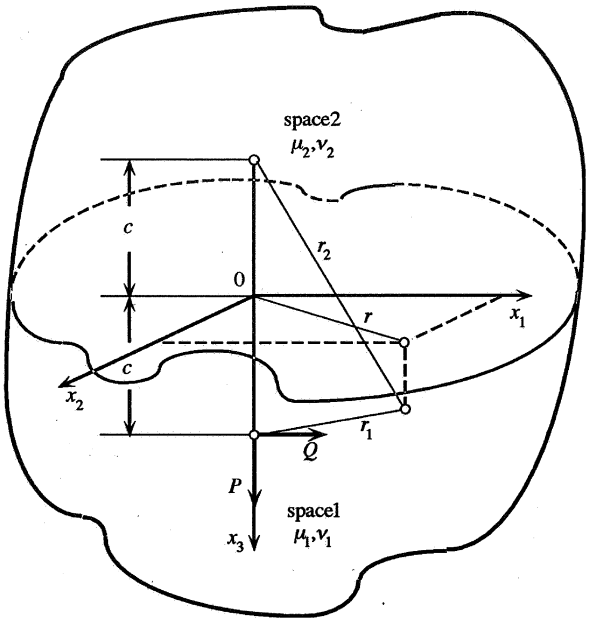

Fig. A.1. Point forces in a bimaterial whose interface is in x_1x_2 plane.

Appendix B. How to derive $K_{ij}^{f_{ij}}$ in Eq. (1a)

Consider a bimaterial as shown in Fig. A.2 whose interface is in the xz^* plane. In Eq. (1a), the notations $K_{ij}^{f_{ij}}$, $K_{zz}^{f_{yz}}$, $K_{zz}^{f_{zx}}$ refers to the stress component σ_{ij} when the standard set of point forces, f_{zz}, f_{yz}, f_{zx} are applied as shown in Eq. (A.10) [20].

$$\begin{aligned} K_{ij}^{f_{zz}} &= \left.\frac{\partial\sigma_{ij}^{R}}{\partial\zeta}\right|_{R=1} + \frac{v}{1-v}\left(\left.\frac{\partial\sigma_{ij}^{Q}}{\partial\eta}\right|_{Q=1} + \left.\frac{\partial\sigma_{ij}^{P}}{\partial\xi}\right|_{P=1}\right) \\ K_{ij}^{f_{yz}} &= \left.\frac{\partial\sigma_{ij}^{R}}{\partial\eta}\right|_{R=1} + \left.\frac{\partial\sigma_{ij}^{Q}}{\partial\zeta}\right|_{Q=1} \\ K_{ij}^{f_{zx}} &= \left.\frac{\partial\sigma_{ij}^{R}}{\partial\xi}\right|_{R=1} + \left.\frac{\partial\sigma_{ij}^{P}}{\partial\zeta}\right|_{P=1} \end{aligned} \tag{A.10}$$

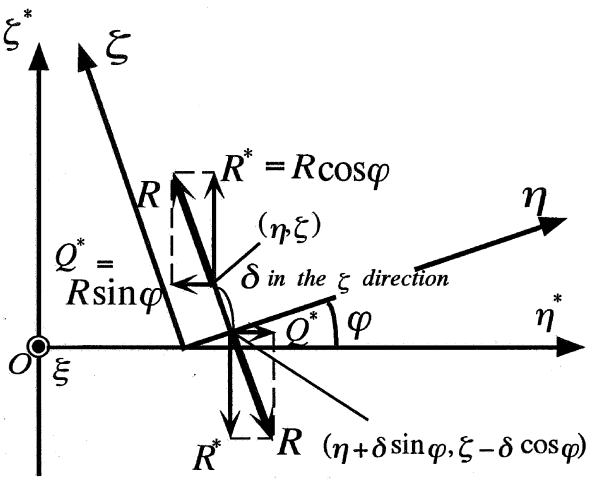

Fig. A.2. How to derive $K_{ij}^{f_{ij}}$.

Here, $\sigma_{ij}^{P}, \sigma_{ij}^{Q}, \sigma_{ij}^{R}$ are the stresses due to point forces P, Q, R acting in the ξ, η, ζ directions. As an example, $\frac{\partial \sigma_{ij}^{R}}{\partial \zeta}$ can be derived in the following way.

$$\sigma_{ij}^{R^*} = R\cos\varphi\sigma_{ij}^{R^*}(\eta^*,\zeta^*,y^*,z^*)|_{R^*=1} - R\cos\varphi\sigma_{ij}^{R^*}(\eta^*+\delta\sin\varphi,\zeta^*-\delta\cos\varphi,y^*,z^*)|_{R^*=1}$$

$$\sigma_{ij}^{Q^*} = R\sin\varphi\sigma_{ij}^{Q^*}(\eta,\zeta,y,z)|_{Q^*=1} + R\sin\varphi\sigma_{ij}^{Q^*}(\eta+\delta\sin\varphi,\zeta-\delta\cos\varphi,y,z)|_{Q^*=1} \tag{A.11}$$

$$\frac{\partial\sigma_{ij}^{R}}{\partial\zeta} = \lim_{\delta\to 0}\left(\frac{\sigma_{ij}^{R^*}+\sigma_{ij}^{Q^*}}{\delta}\right)\left(\left.\frac{\partial\sigma_{ij}^{R^*}}{\partial\zeta}\right|_{R^*=1}\cos\varphi - \left.\frac{\partial\sigma_{ij}^{R^*}}{\partial\zeta}\right|_{R^*=1}\sin\varphi\right)\cos\varphi$$
$$+\left(\left.\frac{\partial\sigma_{ij}^{Q^*}}{\partial\zeta}\right|_{Q^*=1}\cos\varphi - \left.\frac{\partial\sigma_{ij}^{Q^*}}{\partial\eta}\right|_{Q^*=1}\sin\varphi\right)\cos\varphi \tag{A.12}$$

Appendix C. Probable angle θ_0 of crack propagation

Table C.1 show probable angle θ_0 of crack propagation, which are obtained from the condition of maximum σ_θ [27], that is,

$$K_{II}(1-3\cos\theta_0) - K_I\sin\theta_0 = 0, \quad 3K_{II}\sin\theta_0 - K_I\cos\theta_0 < 0 \tag{A.13}$$

Table C.1
Probable angle θ_0 of crack propagation

	h/b	$a/b=1$		$a/b=2$		$a/b=\infty$	
		$-\mu_2/\mu_1=0$	$-\mu_2/\mu_1=\infty$	$-\mu_2/\mu_1=0$	$-\mu_2/\mu_1=\infty$	$\mu_2/\mu_1=0$	$-\mu_2/\mu_1=\infty$
$\varphi=15°$	1.05	−30.0	−28.4	−24.8	−24.5	−23.4	−22.2
	1.1	−29.9	−28.1	−26.4	−24.9	−24.3	−21.6
	1.2	−31.3	−26.5	−28.7	−25.3	−26.5	−22.5
	1.4	−30.4	−26.5	−28.0	−23.0	−26.0	−25.3
	1.6	−30.1	−28.6	−27.9	−26.6	−25.9	−26.2
	2.0	−30.0	−29.8	−28.0	−27.7	−26.0	−26.7
	∞	−30.2	−30.2	−28.4	−28.4	−26.7	−26.7
$\varphi=45°$	1.05	−56.2	−53.8	−54.6	−53.4	−57.0	−53.3
	1.1	−58.0	−53.2	−55.4	−53.4	−51.2	−53.2
	1.2	−59.2	−53.5	−57.1	−54.7	−54.7	−54.2
	1.4	−57.5	−54.9	−55.7	−53.7	−53.9	−54.5
	1.6	−56.7	−55.3	−55.2	−54.1	−53.5	−54.1
	2.0	−56.0	−55.3	−54.7	−54.0	−53.1	−53.6
	∞	−55.5	−55.5	−54.3	−54.3	−53.1	−53.1
$\varphi=45°$	1.05	56.2	53.8	54.6	53.4	57.0	53.3
	1.1	58.0	53.2	55.4	53.4	51.2	53.2
	1.2	59.2	53.5	57.1	54.7	54.7	54.2
	1.4	57.5	54.9	55.7	53.7	53.9	54.5
	1.6	56.7	55.3	55.2	54.1	53.5	54.1
	2.0	56.0	55.3	54.7	54.0	53.1	53.6
	∞	55.5	55.5	54.3	54.3	53.1	53.1
$\varphi=75°$	1.05	28.3	29.7	23.8	23.8	23.3	23.8
	1.1	29.1	27.7	25.9	24.8	24.6	21.8
	1.2	29.9	25.7	27.6	22.6	26.8	21.2
	1.4	29.7	26.5	27.3	20.4	24.2	24.6
	1.6	29.7	27.3	27.3	21.7	24.2	25.6
	2.0	29.7	26.8	27.3	23.5	24.2	26.1
	∞	30.2	30.2	28.4	28.4	26.7	26.7

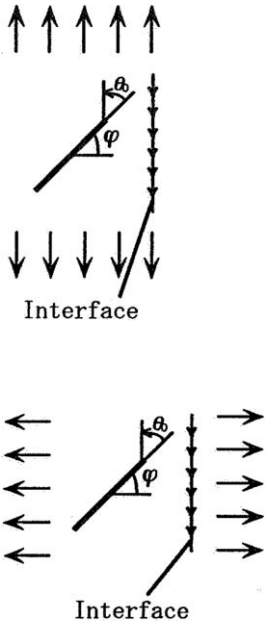

$K_{II}(1-3\cos\theta_0) - K_I\sin\theta_0 = 0$, $3K_{II}\sin\theta_0 - K_I\cos\theta_0 < 0$.

Initially, the crack seems to propagate to the direction θ_0 in Table C.1, and then, changes the direction perpendicular to the tensile direction.

References

[1] Erdogan F, Aksogan O. Bonded half planes containing an arbitrarily oriented crack. Int J Solids Struct 1974;10:569–85.
[2] Cook TS, Erdogan F. Stresses in bonded materials with a crack perpendicular to the interface. Int J Engng Sci 1972;10:677–97.
[3] Isida M, Noguchi H. An arbitrary array of cracks in bonded semi-infinite bodies under in-plane loads. Trans Japan Soc Mech Engrs 1983;49(437):36–45 [in Japanese].
[4] Willis JR. The penny-shaped crack on an interface. Q J Mech Appl Math 1972;25:367–85.
[5] Erdogan F, Arin K. Penny-shaped interface crack between an elastic layer and a half-space. Int J Solids Struct 1972;8:93–9.
[6] Kassir MK, Bregman AM. The stress intensity factor for a penny-shaped crack between two dissimilar materials. ASME J Appl Mech 1972;39:301–8.
[7] Lee JC, Farris TN, Keer LM. Stress intensity factors for cracks of arbitrary shape near an interfacial boundary. Engng Fract Mech 1987;27(1):27–41.
[8] Shibuya T, Koizumi T, Iwamoto T. Stress analysis of the vicinity of an elliptical crack at the interface of two bounded half-spaces. JSME Int J 1989;32:485–91.
[9] Nakamura T. Three-dimensional stress fields of elastic Interfaces Cracks. ASME J Appl Mech 1991;58:939–46.
[10] Yuuki R, Xu J-Q. ABEM analysis of a three-dimensional interfacial crack of bimaterials. Trans JSME 1992;58:39–46 [in Japanese].
[11] Noda NA, Ohzono R, Chen MC. Analysis of an elliptical crack parallel to a bimaterial interface under tension. Mech Mater 2003; 35:1059–76.
[12] Qin TY, Noda NA. Analysis of a three-dimensional crack terminating at an interface using a hypersingular integral equation method. ASME J Appl Mech 2002;69:626–31.
[13] Qin TY, Noda NA. Stress intensity factors of a rectangular crack meeting a bimaterial interface. Int J Solids Struct 2003;40:2473–86.
[14] Noda NA. Stress intensity formulas for three-dimensional cracks in homogeneous and bonded dissimilar materials. Engng Fract Mech 2004;71:1–15.
[15] Noguchi H, Isida M, Tsuru H. New method of analysis of three-dimensional crack problems (2nd Report, application to semi-infinite body problems with an arbitrary surface or internal crack under complex loading conditions). Trans JSME 1993;59(561):1279–86 [in Japanese].
[16] Oda K, Muraoka Y, Noda NA. Analysis of an elliptical internal crack near free surface using singular integral equation of the body force method. Trans JSME 2001;67(664):2025–31 [in Japanese];
Oda K, Muraoka Y, Noda NA. Analysis of an elliptical internal crack near free surface using singular integral equation of the body force method. Key Engng Mater 2001;243–244:375–80.
[17] Noda NA, Miyoshi S. Variation of stress intensity factor and crack opening displacement of semi-elliptical surface crack. Int J Fract 1996;75:19–48.
[18] Noda NA, Kobayashi K, Yagishita M. Variation of mixed modes stress intensity factor of an inclined semi-elliptical surface crack. Int J Fract 1999;100:207–25.
[19] Hadamard J. Lectures on Cauchy's problem in linear partial differential equations. New Haven, CT: Yale University Press; 1923.
[20] Nisitani H, Chen DH. The body force method (Taisekiryokuho in Japanese). Bifukan, Tokyo 1987. p. 39–66;
Chen DH, Nisitani H. Body force method. Int J Fract 1997;86:161–89.
[21] Murakami Y, Endo M. Quantitative evaluation of fatigue strength of metals containing various small defects or cracks. Engng Fract Mech 1983;17(1):1–15.
[22] Kageyama K, Okamura H. Elastic analysis for an infinitesimal kinked crack under tension and in-plane shear, and fracture criterion based on maximum strain energy release rate. Trans JSME 1982;48(430):783–91 [in Japanese].
[23] Nisitani H, Chen DH, Isida M. Evaluation for mixed mode stress intensity factors of several types of cracks emanating from an elliptical hole. Trans JSME 1984;50(451):341–50 [in Japanese].
[24] Noda NA, Oda K. Effect of curvature at the crack tip on the stress intensity factor for curved cracks. Int J Fract 1993;64:239–49.
[25] Chen MC, Noda NA. Force at a point in the interior of one of two jointed semi-infinite solids. In: Proceedings the 2002 annual meeting of JSME/MMD 2003;55-4:468-475 [in Japanese].
[26] Chen MC, Noda NA. Fundamental solution due to a point force in the interior of one of two jointed semi-infinite solids. Kikai Kenkyu (Sci Mach) 2003;55(4):468–75 [in Japanese].
[27] Erdogan F, Sih GC. On the crack extension in plates under plane loading and transverse shear. J Basic Engng, Trans ASME, Series D 1963;85:519–25.